DEVELOPMENT AND CHARACTERIZATION OF REACTIVE EXTRUSION ADDITIVE MANUFACTURING SYSTEM AND POLYMER

A Thesis
Submitted to the Graduate Faculty
of the
North Dakota State University
of Agriculture and Applied Science

By

Dallas Jacob Patton

In Partial Fulfillment of the Requirements
for the Degree of
MASTER OF SCIENCE

Major Department:
Mechanical Engineering

September 2021

Fargo, North Dakota

North Dakota State University
Graduate School

Title

DEVELOPMENT AND CHARACTERIZATION OF REACTIVE EXTRUSION ADDITIVE MANUFACTURING SYSTEM AND POLYMER

By

Dallas Jacob Patton

The Supervisory Committee certifies that this ***disquisition*** complies with North Dakota State University's regulations and meets the accepted standards for the degree of

MASTER OF SCIENCE

SUPERVISORY COMMITTEE:

Dr. Chad Ulven
Chair

Dr. Long Jiang

Dr. Dean Webster

Approved:

November 16, 2021
Date

Dr. Alan Kallmeyer
Department Chair

ABSTRACT

Additive manufacturing with polymers can rapidly produce complex geometry and prototypes but does not usually utilize thermoset polymers aside from photocurable polymers. In this study two-part reactive thermoset resin systems were used to additively manufacture parts utilizing a commercial resin and a custom resin system. Two displacement syringe drivers were used to feed each part of the reactive resin into a mix chamber that utilized a helical static mix rod and was extruded through a 3D printed nozzle. After print parameters were fine-tuned, the resulting reactive resin specimens featured high strength, quick curing, and fast deposition rate. Optimization of the resin system is required to allow for support structures to be created as well as for overhangs and other additive manufacturing advantages to be realized. Continued study on reactive extrusion methods can lead to the utilization of continuous fiber to allow for the creation of complex geometry high performance composites.

ACKNOWLEDGMENTS

First, I would like to thank the Army Research Laboratory for sponsoring this research project. Next, I'd like to thank Dr. Chad Ulven, my advisor and committee chairman. Dr. Ulven's guidance and mentorship allowed me to succeed and was proven to be invaluable throughout this research. Luke Gibbon is another person well deserving of a thanks as he also provided an immense amount of guidance, and leadership on this project. I would like to thank my committee member Dr. Long Jiang for his help in understanding different polymer mechanics and I would like to express thanks to Dr. Dean Webster for his immense knowledge of polymer chemistry that proved to be very useful.

Alexander Hart a PHD student, from NDSU's Coatings and Polymeric Materials Department, provided relevant feedback, a lot of time, and effort to this project. His assistance was invaluable, and this project would have looked very different without Alex on the project. Additionally, I would like to thank the undergraduate researchers for lending a hand in the project wherever was needed.

Finally, I would like to thank all my friends and family who have supported me, you know who you are, and helped me pursue a master's degree. I could not be where I am today without the support of everyone on this list and I will be forever grateful.

TABLE OF CONTENTS

LIST OF TABLES

LIST OF FIGURES

LIST OF ABBREVIATIONS

VARTM .....Vacuum assisted resin transfer molding.

PX .....Pentaerythritol and m-xylylenediamine.

LIST OF SYMBOLS

π .....Pi.

r_1 .....Radius at exit of nozzle.

H .....Head speed rate.

D_1 .....Density of polymer.

a.....Dry mass of the polymer.

b_1.....Apparent mass of the fully immersed polymer.

ρ_W .....Density of water.

E .....Modulus of elasticity.

σ_T .....Tensile stress.

ε_T.....Tensile strain.

R.....Crosshead rate.

L .....Support span.

d.....Depth of beam.

D.....Midspan deflection.

r .....Strain.

σ_F .....Flexural stress.

P .....Load.

b.....Width of beam.

ε_F.....Flexural strain.

E_F .....Chord modulus.

σ_{fn}.....Flexural stress at predefined point

ε_{fn} .....Flexural strain at predefined point.

LIST OF APPENDIX TABLES

LIST OF APPENDIX FIGURES

1. INTRODUCTION

Additive manufacturing, or 3D printing, was first commercially used in 1987 in the form of stereolithography [1]. 3D printing is a rapidly growing mode of manufacturing for both professionals and enthusiasts. 3D printing offers many advantages in the fabrication of composites, including high precision, cost effectiveness and customized geometry [2]. Additive manufacturing can include metals, ceramics, and polymers, however, this study was focused on polymer additive manufacturing. Typically, two forms of polymer 3D printing are used, stereolithography apparatus (SLA) or fusion deposition modeling (FDM). Experiments have been conducted on fiber reinforced 3D printed composites and they can be created from many methods [3]. SLA is a liquid-based process that consists of curing a photosensitive polymer [4]. A new form of additive manufacturing is emerging, which is printing with reactive thermoset resins. 3D printing with reactive thermoset resins allows for the high properties of a thermoset with little to no post curing necessary.

1.1. Thermoset Resin Additive Manufacturing

1.1.1. UV Cured Reactive Resins

A common method of producing thermoset polymers via reactive additive manufacturing is accomplished by utilizing photosensitive polymers. Photosensitive polymers, or photopolymers, are polymers that change physical properties when exposed to UV light [5]. The first resins patented for SLA were published in 1989 and 1990 [6-7]. Initially, parts produced with these polymers were inaccurate and were only cured 46% [8]. Acrylate resins exhibited high reactivity but showed low resulting properties which led to the use of epoxide resins [9]. It was found that epoxy resins experienced lower shrinkage and produced higher modulus parts than acrylate resins [9]. Although epoxy resins created harder and more accurate parts, the epoxy resin system also

produced brittle parts and the print process was slow. For this reason, common resin systems for SLA systems are an epoxide acrylate combination to allow for accurate rapid production with reduced brittleness [10]. Two advantages of UV cured reactive resins in vat-based photopolymerization techniques are accuracy and surface finish [8]. Given that laser irradiance depth and scan patterns have been optimized, the layer height of SLA systems can be as small as 25 microns to allow for excellent surface finish and part accuracy by reducing the gradient between steps [8]. The biggest drawback of vat-based photopolymerization techniques is that the resin systems used have mechanical properties that degrade over time due to aging as well as low impact strength [8]. Another drawback is in the process itself, if the laser is inhibited in anyway, like an obstructed optical window, the resulting part will not be able to optimally cure and thus results in low print quality.

1.1.2. Epoxy Resins

Many groups of reactive resins exist, some of which are epoxy functional resins, phenolic resins, and polyurethane resins. Epoxy functional resins are crosslinked by mixing the epoxy with curing agents [11]. An oligomer containing two or more epoxide groups make up the epoxy side [11]. The curing agent or hardener is usually an amine compound or a diacid compound [11]. Epoxy resins are used for many processes, but one process known as Vacuum Assisted Resin Transfer Molding (VARTM) is a low-cost method to create large composite specimens [12]. VARTM is a liquid composite molding technique that pulls resin through a fiber layup section by using a vacuum to assist in resin transfer through the part. Given that an epoxy resin can have a longer pot life than other polymers, it is used in this process to allow for the resin to wet out the fiber layup prior to gelation.

Epoxy is used in many other processes and industries as well including adhesives, wind turbine composites, and high-performance vehicles applications. Epoxy adhesives, commonly referred to as structural adhesives, have high strength bonds and are used in repairs or construction of bicycles, golf clubs, snowboards, and many more [13]. Epoxy resin has been used to create complex parts via reactive extrusion additive manufacturing [14]. Uitz et al. used EPON 8111 epoxy resin from Hexion Inc.® mixed with EPIKURE 3271 curing agent also from Hexion Inc.® with a volumetric mix ratio of 4:1 [14]. Fumed silica by E K Industries Inc. ®, CAS No. 112945-52-5 was added at 3.5% by weight to increase the viscosity of the resulting resin. The gel time for this epoxy was 1 minute which helped support additional layers without much deformation. A cool down-period was required before removing parts from the bed because the resin featured an exothermic polymerization reaction. Specimens were created by a 6-layer high specimen that was then cut to size along parallel or perpendicular orientation to the raster direction. The specimens were cut and surfaced using a CNC milling machine [14].

1.1.3. Phenolic Resins

Phenolic resins result from the reaction of formaldehyde and phenol and are the first truly synthetic commercially available plastic resin [15-16]. Like many other polymers, phenolic resins have a wide range of applications some of which include ballistics, mass transit, and electronics. Phenolic resins have low thermal conductivity, low density, and high strength to weight ratio among other things [17]. When phenolic resin is combined with Aramid fibers, it creates a strong and tough composite with high impact resistance making it great for ballistic protection applications [18]. Dimeski et al. studied the effect of phenolic Aramid composites under ballistic impact and found that when the composite has 20% resin content the composite performs better than a composite with 50% resin content [18]. Hubert et al. blended phenolic resin with neoprene

rubber to create thermally stable adhesives [19]. Mass transit vehicles, buses, and trains, have strict fire safety requirements making the phenolic neoprene polymer blend a good candidate for use in the mass transit industry [20].

Additive manufacturing has been completed using phenolic resins. Masuda et al. combined silicon carbide with phenolic resin and extruded it in an FDM style 3D printer [21]. Without fillers phenolic resins are prone to shrinkage and brittleness [16]. To cure the specimens heat flow from the bed was used, to increase the effect of the heated bed, the thermal conductivity of the resin system was of interest. The volume fraction of silicon carbide used was 53% and water was also added to reduce the viscosity as it was too high to dispense. The dispense method was performed via displacement pump on a syringe. The 3D printer was able to produce spiraled hollow geometry that allowed for the use of other heaters to help cure the part.

1.1.4. Polyurethane Resins

Finally, polyurethanes, which are formed by reaction between isocyanate and polyols [22]. The reaction to produce polyurethanes can take place by mixing the two reactants which forms a urethane linkage. A benefit of polyurethanes is that it is not a condensation polymerization which would generate water [16]. Polyurethanes can be tailored for specific mechanical properties. Generally, they are elastic materials with high toughness. However, polyurethanes can be adjusted from high elongation and high energy absorption to have a high elastic modulus and high strength. The mechanical properties can be adjusted by changing the aromatic content of the monomers within the urethane [16].

Polyurethanes and polyureas have similar components. Polyurethanes are created by combining isocyanates and polyols. Whereas polyureas are created by combining isocyanate with multifunctional amines. Additionally, a hybrid of these two polymers can be created by combining

isocyanate with a mixture of polyol and amino groups to provide a blend of characteristics [16]. Specialty Products Inc. features a variety of polyurea with gel times from as low of 5 seconds to up to 9 min [23], [24]. Additionally, the polyurea were 100% solid, and cure at room temperature with no post curing necessary. Kokkinis et al. utilized polyurethane acrylate ink with magnetically responsive particles [25]. A two-component mixer and dispenser were integrated into a 3D printing gantry system. The printer was able to create complex helical structures among other geometry.

1.1.5. Mixing and Dispensing Options

Proper mixing of a two-part polyurethane or polyurea system is crucial. Without an ideal mix the polymer will not be able to fully crosslink and will have reduced mechanical properties [26]. Mixing of the polymer can be performed in different ways, such as impingement, dynamic, and static mixing. Impingement mixing is where two high velocity streams collide with one another and mix during the turbulent flow [27]. Impingement mixing provides a homogenous mix but requires a high velocity between the two fluids which can increase the capital equipment cost. Dynamic mixing can consist of a paddle and a motor, the motor drives the paddle and mixes the polymer. Dynamic mixing can provide a homogenous mixture of high viscosity systems; however, it is an expensive option especially for large scale projects. Static mixing has a low cost because it contains no moving parts and only requires an inline mixer. However, additional costs come from flow metering equipment to control the volume dispensed. The mixer consists of a certain number of elements that create laminar flow and produce irregular paths for the fluids [28].

Static mixing has many advantages, some include flow, cure, and cost [29]. Static mixing can be used for high viscosity fluids when other mixing options are not applicable. Static mixing does not require high fluid velocity because the mix design consists of mixing elements that are offset 90° from the previous element. This offset disrupts the path of the fluid and causes both

fluids to fold over one another until they are homogenously mixed. Shown below, Figure 1, depicts a helical static mix rod that is designed to be used for this experiment, it features 16 6.25 mm mixing elements in a 101.6 mm section.

Figure 1. Helical static mix rod.

Uitz et al. and Rios et al. created reactive resin extrusion 3D printers [14], [30]. Rios et al. utilized two volumetric dosing pumps which feed each component into the mixing nozzle. Volumetric dosing pumps work by having a fluid flow into a chamber with an automated screw that dispenses the liquid at a certain volumetric rate [30]. Each extruded material exhibited a long cure time that allowed for a continuous network of chemical cross-links throughout the part. Uitz et al. utilized two twin piston positive displacement pumps that would dispense two-part reactive resin into a Sulzer Mixpac MS 10-18 T, 214 mm long, and 10 mm inner diameter mix nozzle [14]. Successive layers are deposited and cured rapidly *in situ* that required no external energy. Uitz analyzed the effect of orientation on mechanical properties.

1.2. Reactive Resin Additive Manufacturing and Composites

Volumetric dosing pumps are used in a variety of industries such as medical technology, adhesives, soldering pastes, cosmetics, and the food industry [31]. ViscoTec creates volumetric dosing pumps that allow for materials with viscosity up to 7 kPa*s to be dispensed. Volumetric dosing pumps utilize a progressive cavity pump, which consists of fluid passing through a small sequence of shapes as a rotor is turned. Two-component progressive cavity pumps have been used in bioprinting and 3D printing that incorporates mechanical gradients to produce composite

specimens [25, 32-33]. Additionally, a single component progressive cavity pump has been used to additively manufacture concrete structures [34].

Rios et al. is one of few articles found in the field of reactive resin extrusion additive manufacturing, another similar study was performed by Uitz [14]. Uitz featured a reactive extrusion additive manufacturing methodology like Rios but analyzed the alleged isotropic properties of a print as well as the thermodynamic nature of the exotherm process. The isotropic properties in the tensile direction were reported regardless of print orientation. Only the modulus and ultimate tensile strength showed isotropic results but the elongation at break and toughness were orientation dependent. The printer used by Uitz. featured a 214 mm inline helical static mixer and the resin used was a shear thinning epoxy that cured via in situ epoxidation [14].

Compton and Lewis completed a study on 3D printing of lightweight cellular composites, featuring an FDM style printer [35]. This study features an epoxy-based ink with silicon carbide to create hierarchical structures inspired by balsa wood, yielding an increase of Young's Modulus up to 10 times higher than commercial additive manufacturing thermoplastics. Additionally, the cellulose composite retained comparable strength values 71.1 ± 5.3 MPa. Silicon carbide and carbon fibers were used as fillers aligned in the printing direction. Each filler displayed pullout in the longitudinal specimens and minimal pullout in transverse specimens. Although this study revealed an increase in Young's Modulus, it is expected that continuous carbon fiber will provide higher mechanical properties than the discontinuous fiber that was used in the Compton and Lewis study [35].

2. OBJECTIVES

After review of available literature, referenced in Sections 1.1 to 1.2, there is little available literature and data on the mechanical properties of reactive extrusion additive manufacturing. The purpose of this research is to develop a 3D printing reactive extrusion method, that requires no post cure procedure, and to evaluate the resulting specimen's mechanical properties. The future of this research dictates that a 3D printer be used with as little procedure as possible. This resulted in the goal of creating an additive manufacturing method that requires no post cure procedure. To accomplish this, the following objectives have been created:

- Develop a reactive extrusion additive manufacturing system that can produce different polymer specimens capable of being mechanically tested.
- Evaluate and compare the mechanical properties of the cast and printed versions of each polymer system.

3. RESEARCH METHODOLOGY

3.1. Polymeric Material

Two resins will be comprehensively evaluated, one is commercially available through Specialty Products, EPL™ 4 (Lakewood, Washington). EPL 4 is a self-leveling polyurea elastomer created to repair material cracks such as warehouse floors or decks. Table 1 depicts some of the advertised properties of EPL 4 [36]. The EPL 4 polyurea was selected because it was developed to be statically mixed or sprayed and possessed a curing profile that includes a 4-minute gel time, which is desired for dispensing. Initially, mechanical properties of commercial resins were not considered, pot life was the most important parameter considered. The EPL 4 features 100% solids and is not a condensation reaction. A 100% solid material was ideal because it allowed for the assumption that each layer deposited on top of one another produced a uniform cross section. The second resin was developed by NDSU's Coatings and Polymers Department. The experimental resin was tailored for pot life, viscosity, and post cure procedures best suited for the systems developed. The resulting polymer system selected was a polyenamine system produced via a condensation reaction, which does not produce any volatile organic compounds [37].

Table 1. Specialty Products EPL 4 Properties [36].

Tensile Strength (MPa)	Elongation (%)	Modulus (MPa)	Pot Life (min)
16	245	6	4

4. SAMPLE MANUFACTURING

4.1. Casting Neat Baselines

While the commercial resin, EPL 4, has published mechanical properties, the resin was cast to generate a set of baseline mechanical properties using the same test parameters in this study. The molds were cast Smooth-On Mold Star^{TM} 15 Slow silicone that was poured over a stainless-steel die of exact geometry for tensile and flexural testing. To create a baseline of properties to compare printed samples against, an impeller mixer was used at a 1000 rpm for 30 s to create EPL 4 cast specimens. No degassing was possible for the EPL 4 as the system cured quickly and did not foam upon starting the exothermic reaction. Foaming could occur if the exothermic temperature reached high enough to vaporize the polyol resin. Each mold was filled by pouring the homogeneously mixed resin system from a beaker and then a weighted plate was placed on top of the molds to ensure each specimen was flat and resulted in a uniform cross section. Without having a weighted plate on top of the molds, the EPL 4's surface tension would create a rounded surface on the top. Additionally, the experimental resin created by NDSU's Coatings and Polymeric Materials Department was hand mixed for 15 s until the resin started to exotherm then it was poured into silicone molds. The system required a section of the material to be restrained for uniform flat parts but needed other area to be unrestricted and allowed to foam. The tensile specimens featured restriction in the gauge area and the grip section was free to foam. The flexural specimens were sanded down to flat sections removing the excess resin that created a curved structure as well as the grip sections of tensile specimens were sanded. Each resin system cured in the mold at room temperature for 24 h before being removed from the molds and continued to cure for at least a total of 72 h before testing. No post-curing was performed as the resin systems were designed to cure over a 72 h period at room temperature.

4.2. Printing

The specimens were printed directly to the specific geometry per each test ASTM standard. This was performed because the machineability of elastomers is very low and to prove that a part can be printed using this approach. It was expected that the 3D printed specimens would have lower layer adhesion and resolution than the cast specimens because the cast specimens would be deposited entirely at once and the printed specimens were deposited layer by layer. Another reduction in properties was expected because low print resolution causes stress concentrations that would cause premature failure. For these reasons it was expected that the 3D printed specimens would have lower mechanical properties than the cast specimens. The specimens were oriented to print with the lowest overall height to allow the bed to support each print. The bed supported the resin and the resin flowed less than if it was being supported by a small section of the printed specimen.

4.2.1. Equipment Setup

The equipment used to create the custom mix chamber consisted of an aluminum pipe, two threaded brass barbed tube fittings, and a stainless-steel wye connector. The material selection was dictated by the need to burn off and clean the mix chamber components while structural integrity remained intact. PVC plastic tube was connected from the syringes to the barbed tube fittings. The sections of PVC plastic tube were of similar length to ensure each tube experienced similar expansion in the lines. Each barbed fitting threaded sections and each threaded end of the aluminum pipe were wrapped in Teflon to ensure a seal was made at each connection. Figure 2 depicts the Solidworks CAD model of the mix chamber setup.

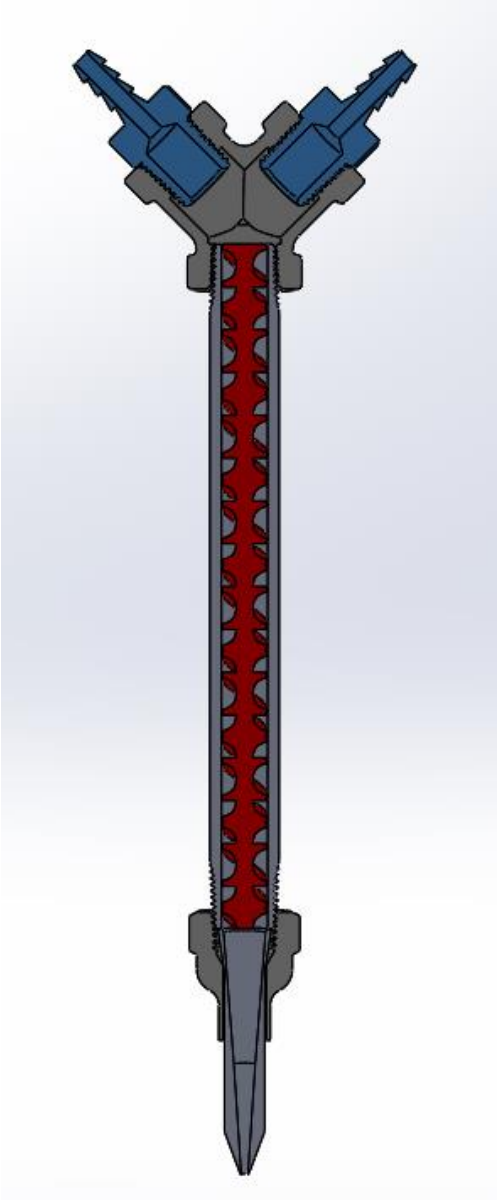

Figure 2. Mix chamber setup with 152.4 mm pipe.

The biggest advantages of static mixing are the low cost and maintaining laminar flow. Other mixing options require equipment to either increase the velocity of the fluid, or to drive the mixing rod to provide an improved mix. To scale up static mixing in industry, the size of the static mix rod increases with the size of pipe used. Depending on the application, static mixer components can be added or removed to integrate into the end user's housing design [38].

Additionally, the static mixer can be tailored for low pressure drop or low-low pressure drop applications [39].

The 50 mL syringes featured quick-turn connectors that were made from polypropylene to withstand the amine side of the polymer system. Two displacement-based syringe drivers were used to dispense each part of the reactive resin system. Each syringe driver featured a control box that could tailor the displacement speed from 0.01 mm/h to as fast as 2.00 mm/s. The syringe drivers were able to fit syringes from 10 mL to 60 mL. However, the syringe drivers were displacement driven, to determine the rate that needs to be dispensed, the distance needed to dispense 1 mL was recorded and used to create the volume to displacement conversion.

The printer used was an ADIMLab Gantry Pro 3D Printer (Shenzhen, China) and it was selected because of its bed size, and open-source software. The bed size of the printer was larger than other printers of comparable price, it features a 310 mm by 310 mm build plate, and it has a maximum height of 410 mm. To protect the print bed from any damages, an aluminum plate of the same size was used to print on. Additionally, the aluminum plate required masking tape be applied to it to allow for the easy removal of printed specimens. The printer's preferred software is Repetier-Host, Hot-World GmbH & Co. KG, Germany, which allowed for each print parameter to be adjusted as needed. It was necessary to control the feed rate as well as having the ability to turn off and remove the heated extruder nozzle while still being able to print. Repetier-Host also features a print preview that allows the G-code to be reviewed prior to printing to ensure the print path is correct as well as five manual control buttons that can be customized with 1000 lines of G-code.

4.2.2. CAD Modeling/Slicing/G-code Work

Directly printing test specimens requires the printer to have a resolution fine enough to accurately deposit samples. The ADIMLab gantry featured position accuracy up to 0.01 mm in X and Y plane and 0.04 mm in the Z direction. Given that the gantry positioning accuracy is far higher than what was needed, the nozzle, flowrate, and G-code needed to be tailored to improve print accuracy. To accomplish this, the CAD models of the specimens needed to account for the resin build up on any edges of the print. Resin build up at each turn on the print was a result of the printer's inability to maintain a constant speed. The print head velocity decreases when it turns which delivers an inconsistent amount of resin. Additionally, as the resin was deposited, the resin continued to flow and flatten out to a width larger than the nozzle outlet diameter. To account for this, G-Code was manually written for each test specimen. G-code is the language 3D printers and other manufacturing machines read. G-code is read as a coordinate system, specifically an X-Y-Z coordinate system, where the Z direction is the build thickness [40]. To print flexural specimens, the X space between layers is written with a MATLAB code that allows for a Y length of 150 mm.

4.2.3. Process Design

Changes between resin systems required adaptations to the mix chamber as well other components. The changes made to the mix chamber included a variable length mix chamber, variable length helical static mix rod, variable speed syringe driver, and a variable nozzle design. First the change in mix chamber length allowed more mix elements. With the helical static mix rods being produced via additive manufacturing, this allowed for the number of elements and overall length to be tailored to the resin system that was used. Figure 3 depicts the engineering drawing of the helical static mix rod including its range of mix elements. Sixteen mix elements were used to print the EPL 4 resin, and 40 mix elements were used to print the custom resin system.

Each mix element measured was 6.25 mm in length, width, and height and are offset 90° rotationally from the previous mix element to ensure the fluids fold over one another. Each helical static mix rod was created using Formlabs (Sommerville, Massachusetts) Clear Resin on the Form 2, with a resolution of 50 μm, which is an SLA style printer.

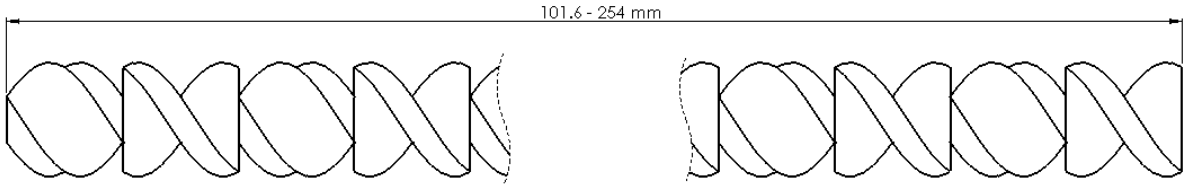

Figure 3. Variable length static mix rod.

To calculate the ratio used between the syringe drivers flow rate and the print head speed, Equation 4.1 was used. The volumetric flowrate was calculated for the mix chamber side and was arbitrarily set for the syringe drivers' side, r_1 is the radius of the exit nozzle, then the head speed rate, H, was determined.

$$\pi {r_1}^2 H = 200 \frac{mm^3}{sec} \quad \text{(Eq. 4.1)}$$

The nozzles were produced by the Form 2, the same printer used to create the mix rods, with 50 μm print resolution and allowed for a change in nozzle diameter without changing any other portion of the geometry. Increasing the diameter of the nozzle allowed for a reduction of mix chamber pressure and allowed for a higher viscosity resin to flow out without syringe driver failure. The smallest diameter possible was desired to produce a high print resolution. A section view of a 1 mm and 3 mm nozzle is depicted below in Figure 4.

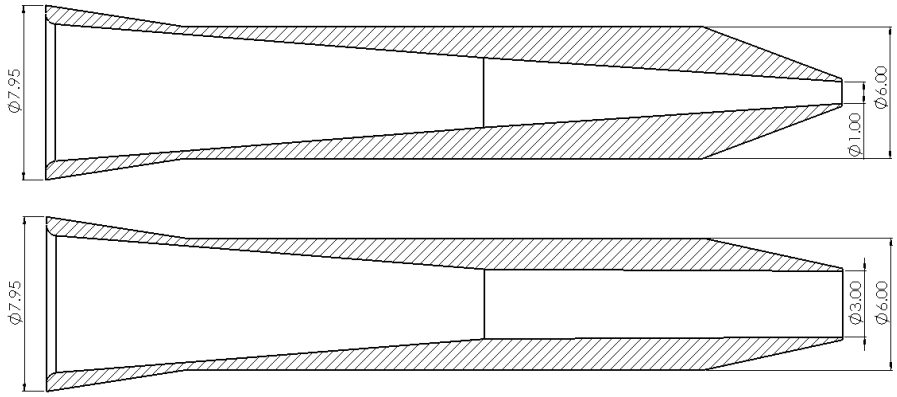

Figure 4. 1 mm nozzle cross section on top and 3 mm nozzle cross section on bottom.

The nozzles were designed to linearly taper down from 6.25 mm to either 1 mm or 3 mm. Additionally the length of the nozzle is enough to allow for tight fit on the mix chamber outlet and reduce the area of stagnant flow which can be problematic with reactive resins.

4.2.4. Qualitative Results

The selection process to provide feedback to the Department of Coatings and Polymeric Materials of the custom resin system used qualitative parameters; these included, speed of dispensed volume, gel time without a post cure, flow of extruded bead while adhering to desired print geometry, and the overall solidification of a finished print. First, the speed from inlet to outlet of the mix chamber was determined by doing a volumetric flow rate calculation and through experimentation. It was found that the time spent in the mix chamber effected the possibility of producing a print. This was because the resin systems used featured a very quick gel time and would gel inside the mix chamber if too much time was spent in the mix chamber. Additionally, each time the speed of the syringe driver was adjusted, the feed rate was also adjusted to maintain the ratio found in Equation 4.1.

Once a resin system was able to flow through the mix chamber without causing the syringe drivers to fail, then the next stage of the print was able to be evaluated. The syringe drivers would

fail either by too much torque needed to continue to dispense the syringe, or the resin would become pressurized in the line and leak from the inlet barbed tube fittings. Observing whether the dispensed material flowing through the system produced a high or low viscosity material was imperative. Viscosity needed to be low enough to flow through the mix chamber with little resistance. However, viscosity then needed to be high enough upon exiting the nozzle to maintain the print shape and have a high print resolution. High viscosity allows for layer buildup and controlled placement. The two parts of the resin system needed to have low viscosity before mixing to reduce the required torque of the syringe drivers. Initially, the print resolution was not of concern and was evaluated after a resin system was developed that could flow through the mix chamber.

Once a resin system was able to successfully dispense through the mix chamber, then the excess flow of the resulting print bead needed to be corrected. Excess flow is the result of a low viscosity material printed on the bed that continued to widen and flatten as it cured. The resin system selected needed to be a low viscosity material inside the mix chamber and increase in viscosity as it exits or shortly after exiting the nozzle. If the resin system was too low in viscosity the printed lines would continue to flow, lowering the overall print resolution as observed in printing with the EPL 4 and shown in Figure 5 below. Finally, once a system was developed that provided a print with similar geometric characteristics, with little to no excess flow, the Department of Coatings and Polymeric Materials tailored the modulus of the resulting print polymer. A Keyence VHX-7000 (Itasca, IL) was used to capture the image in Figure 5.

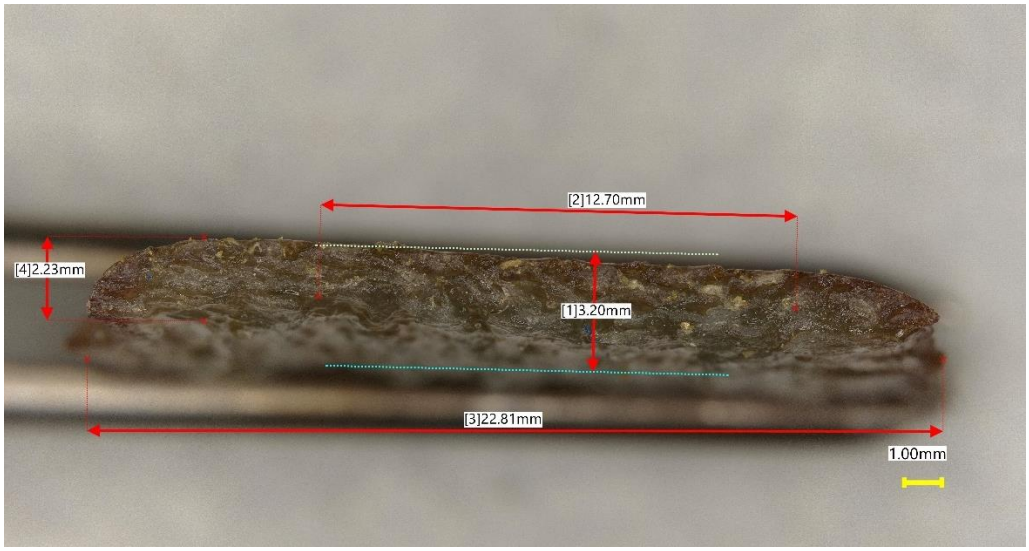

Figure 5. EPL 4 flexural cross section showing excess flow.

An undesirable resin system produced a geometry with close representation to the G-code but was unable to gel, be dry to the touch, or exhibited a low modulus and thus needed to be changed. After multiple trials of finding solutions to materials gelling and being dry to the touch, it was found that the modulus of the resulting print was not high enough to support its own weight when cantilevered. After a material achieved a high enough modulus, and was able to follow the previously required parameters, then it qualified as a potential material. The resulting useable material was pentaerythritol and m-xylylenediamine, here to referred as PX, with a volumetric mix ratio of 1.125 to 1, respectively.

Multiple resin systems needed to be evaluated before the EPL 4 and PX resin systems were selected. Initially, another commercial resin system was selected for the short gel time. It was found that the gel time, of the old commercial system, was too fast to be able to be dispensed. After the commercial resin was selected then the custom resin system was selected. In total, 18 systems were evaluated, and a cumulative list is depicted in Table 2. The X in Table 2 depicts the level that the custom resin was able to complete. Figure 6 exhibits the system diagram used to determine a useable resin system.

Table 2. Cumulative list of trial resins.

Resin System	Part 1	Part 2	1	2	3	4
Specialty Products	Polyshield HT 100F A	Polyshield HT 100F B	X			
Custom 1	30% Glycerol & 70% Sucrose	DETA 1768 2:1	X			
Custom 2	30% Glycerol & 70% Sucrose	DYTEKA 1768 1:3	X	X		
Custom 3	30% Glycerol & 70% Sucrose	DYTREKA 1769	X			
Custom 4	30% Glycerol & 70% Sucrose	Ancamine 1769	X			
Custom 5	30% Glycerol & 70% Sucrose	Ancamine 2071	X	X		
Custom 6	30% Glycerol & 70% Sucrose	DYTEKA Ancamine 2071 1:3	X			
Custom 7	30% Glycerol & 70% Sucrose	DYTEKA Ancamine 2071 1:3 & 2% TEA	X	X		
Custom 8	30% Glycerol & 70% Sucrose	2% Guiacol DYTEKA 2071	X	X		
Custom 9	50 % Glycerol & 50% Sucrose	DYTEKA 2071	X	X	X	
Custom 10	70% Glycerol & 30% Sucrose	2009 HSF DYTEKA 1:3	X			
Custom 11	70% Glycerol & 30% Sucrose	2007 5% TEA	X	X	X	
Custom 12	70% Glycerol & 30% Sucrose	2007 DYTEKA 1:3	X			
Custom 13	70% Glycerol & 30% Sucrose & 2% Guiacol	DYTEKA Ancamine 2071 1:3	X	X		
Custom 14	70% Glycerol & 30% Sucrose & 2% Guiacol	DYTEKA Ancamine 2071 1:3 2% TEA	X	X		
Custom 15	AH-10K Pentaerythritol	DYTEKA Ancamine 1:3	X			
Custom 16	AH-10K Pentaerythritol	2007 5% TEA	X	X	X	
Custom 17	AH-10K Pentaerythritol	3-Cyclohexanebis(methylamine)	X			
Custom 18	AH-10K Pentaerythritol	Furandiamine	X	X	X	

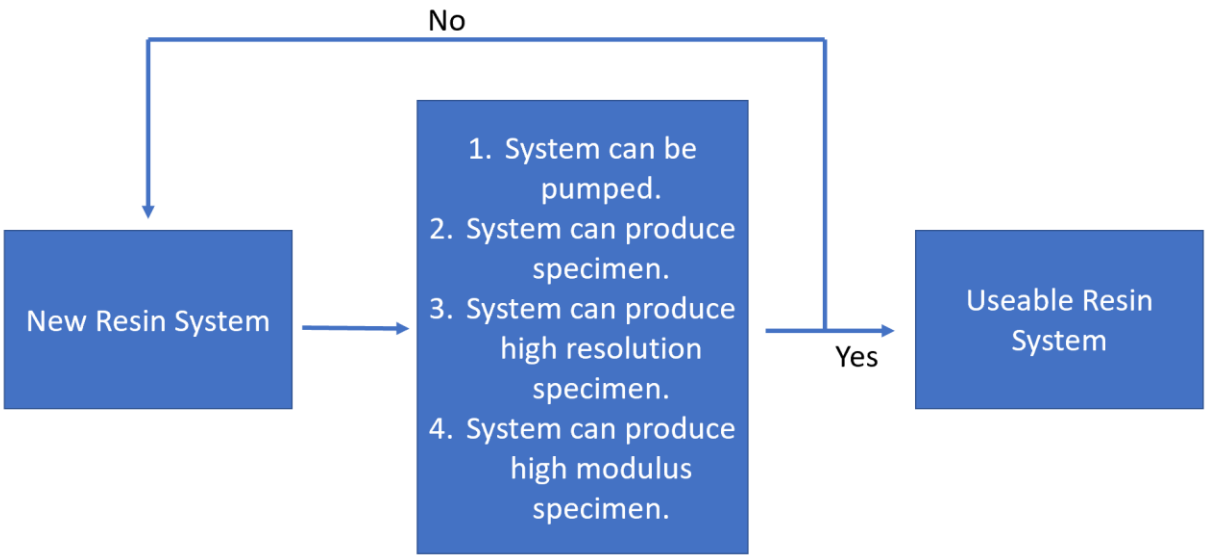

Figure 6. System diagram of resin system.

5. TESTING

5.1. Density

ASTM D792 Method A was followed to test for density of each cast and printed versions of the resin systems [41]. An Ohaus Adventurer^{TM} scale AR2140 (Parsippany, New Jersey) and a Mettler Toledo Density Determination Kit 33360 (Greifensee, Zürich Switzerland) were used in conjunction with a beaker of distilled water and Equation 5.1 was used to calculate density. Where D_1 is density, a is the dry mass of the polymer, b_1 is the apparent mass of the completely immersed specimen and ρ_W is the density of water at 20.4 °C. The density of water at 20.4 °C is 998.15 kg/m^3. First the apparent mass of the specimen was found, the specimen was left on the scale for 5 min to balance out before recording mass and removing. After the apparent mass of the specimens were recorded, the apparent mass of the completely immersed specimens needed to be measured. To measure the apparent mass of the completely immersed specimens the dry specimen was put on the specimen holder and submerged in the immersion vessel. Again, the specimen was left undisturbed for 5 min before recording the apparent mass of the completely immersed specimen completely. Figure 7 below depicts the PX printed specimen inside the apparatus.

$$D_1 = \frac{a}{a-b_1} * \rho_W \quad \text{(Eq. 5.1)}$$

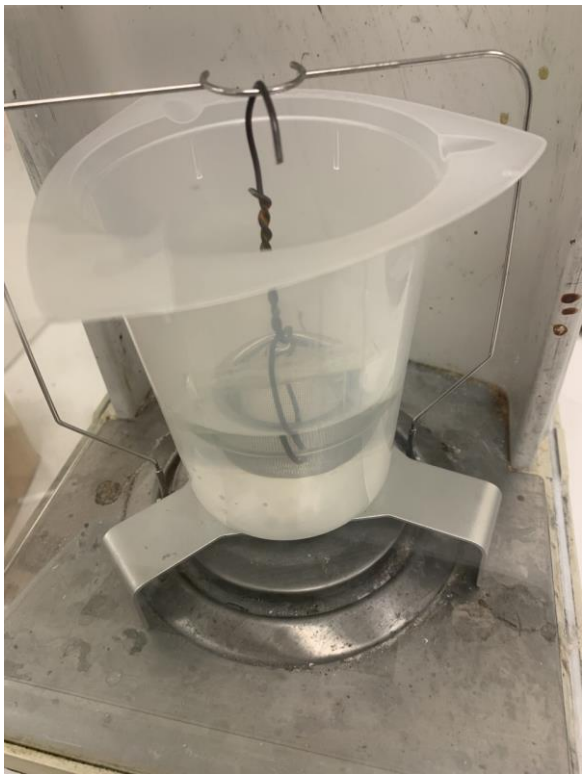

Figure 7. Density test setup featuring PX printed specimen.

5.2. Tensile

An Instron 5567 load frame (Norwood, Massachusetts), equipped with a 2 kN load cell, was used to test tensile properties of the specimens. A 25.4 mm extensometer was used on all cast specimens, however the extensometer values needed to be divided by 50.8. This was because the test input read the extensometer as a 50.8 mm extensometer rather than a 25.4 mm extensometer. An extensometer was not used, on the printed specimens, to monitor strain because securing it to the specimens would cause premature failure by introducing a stress concentration in the gauge section. Strain was calculated by dividing the extension by the gauge length. The ASTM standard referenced for tensile testing was ASTM D638. The crosshead rate of the load frame was set at 5 mm/min. The specimen sizes were type IV for the neat resin specimens and dimensions are in mm. Equation 5.2 and a minimum of 5 specimens of each type was used per the standard [42]. Type IV is meant for nonrigid plastics and dimensions are shown below in Figure 8.

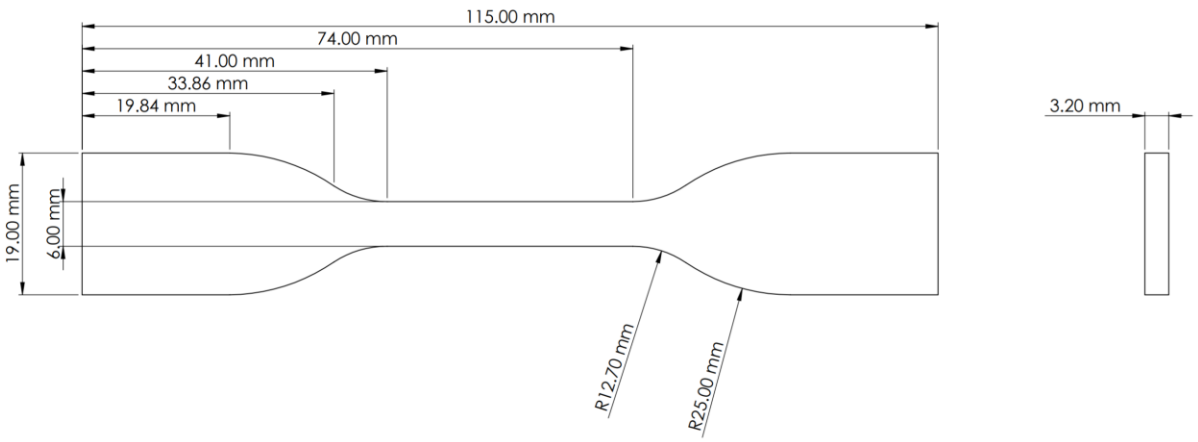

Figure 8. Type IV tensile specimen dimensions.

Modulus of elasticity of the specimen was calculated by Equation 5.2, where E is the modulus of elasticity, σ_T is the tensile stress, and ε_T is tensile strain. The tensile stress and tensile strain values should be taken from the linear portion of the stress-strain curve.

$$E = \frac{\sigma_T}{\varepsilon_T} \quad \text{(Eq 5.2)}$$

The Instron 5567 load frame setup for tensile testing is shown in Figure 9 below. Tensile testing was completed to find engineering tensile strength and strain to failure. Each specimen was preloaded with approximately 1 N to ensure the specimens were in tension prior to testing.

Figure 9. Instron 5567 load frame tensile setup.

5.3. Flexural

Flexural testing was performed to determine flexural strength, and flexural modulus. The flexural test procedure was completed in accordance with the ASTM D790 standard. The test utilized an Instron 5567 load frame, equipped with a 2 kN load cell. Since the specimens were neat, and did not contain reinforcement, 3-point bend flexural testing was concluded at 5% strain or failure per the standard [43]. The crosshead rate was calculated from Equation 5.3. Figure 10 below depicts the specimen dimensions in mm. At least 5 specimens per resin system were tested per the standard.

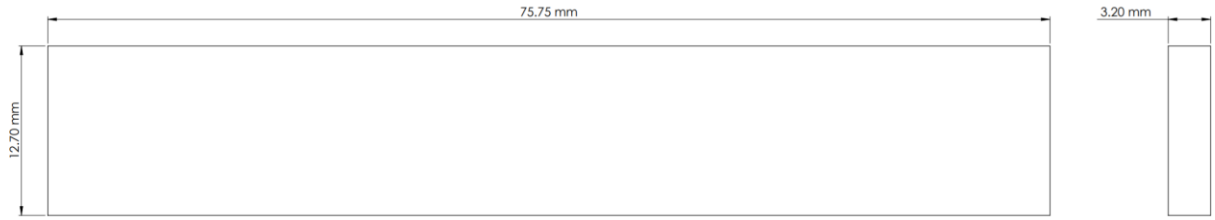

Figure 10. Flexural specimen dimensions.

Crosshead rate was calculated using Equation 5.3, where R is crosshead rate, L is support span, d is depth of beam, and Z is rate of straining of the outer fiber. Z was equal to 0.01 per the ASTM standard.

$$R = \frac{ZL^2}{6d} \quad \text{(Eq. 5.3)}$$

The theoretical deflection at which 5% strain will occur was calculated from Equation 5.4. D is the midspan deflection, r is strain, L is support span, and d is depth of the beam.

$$D = \frac{rL^2}{6d} \quad \text{(Eq. 5.4)}$$

The theoretical midspan deflection was calculated to be 14.94 mm. Flexural stress was calculated from Equation 5.5. Where σ_f is stress in the tension section of beam at midpoint, P is the load given at a point on the load-deflection curve, L is support span, b is width of beam, and d is depth of beam.

$$\sigma_f = \frac{3PL}{2bd^2} \quad \text{(Eq. 5.5)}$$

Flexural strain was calculated from Equation 5.6, where ε_f is strain in the outer surface, D is maximum deflection of the center beam, L is support span, and d is depth of beam.

$$\varepsilon_f = \frac{6Dd}{L^2} \quad \text{(Eq. 5.6)}$$

Chord modulus was calculated from Equation 5.7, where E_f is the chord modulus, σ_{f1} and σ_{f2} are flexural stresses measured at predefined points on the load-deflection curve, and ε_{f1} and ε_{f2} are flexural strains measured at predefined points on the load-deflection curve. The Instron 5567 setup for 3-point bend testing is depicted below in Figure 11.

$$E_f = \frac{\sigma_{f1} - \sigma_{f1}}{\varepsilon_{f2} - \varepsilon_{f1}} \quad \text{(Eq. 5.7)}$$

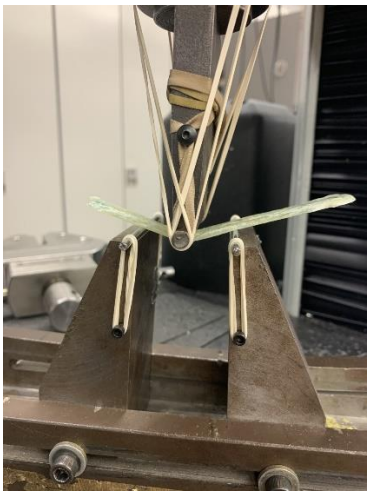

Figure 11. Instron 5567 3-point bend setup.

5.4. Thermogravimetric Analysis

Thermogravimetric analysis, TGA, of the specimens was completed in reference to ASTM D3850 and used nitrogen [44]. Testing was performed on a TA Instruments TGA Q500 (New Castle, Delaware) to determine the thermal degradation temperature for each resin system. Thermal degradation temperature was required before performing differential scanning calorimetry, DSC. This was because DSC test equipment can be damaged if the specimen degrades

while being tested. TGA was executed in conjunction with NDSU's Department of Coatings and Polymeric Materials and Research and Creativity Activity Department. The TGA apparatus is shown in Figure 12 below.

Figure 12. TGA Q500.

5.5. Differential Scanning Calorimetry

Differential scanning calorimetry, DSC, was performed using a TA Instruments DSC Q1000 (New Castle, Delaware) and in reference to ASTM E2160 [45]. An empty tray was weighed and compared to each of the specimens by determining the difference in energy absorption through temperature change. DSC was completed to determine the glass transition temperature, and degree of cure of the polymer. A lower glass transition temperature indicates a lower amount of cross-linking and requires a colder temperature to keep unlinked polymer chains out of their free state [16]. Degree of cure was important to prove the homogeneity of the mixture completed by the static mixing rod during the printing process. DSC was completed three times for each type of specimen. The DSC apparatus is shown in Figure 13 below.

Figure 13. DSC Q1000.

6. RESULTS AND DISCUSSION

6.1. Density

The specimens sank once fully immersed in distilled water which negated the use of a sinker. Density testing was completed for each specimen of both resin systems. The temperature of the distilled water was 20.4 °C and the immersion vessel was a 400 mL beaker. Specimens were prepared by being cut to a small enough size to fit on the sample holder. Table 3 depicts the density values of PX and EPL 4 cast and print specimens. Equation 5.1 was used to determine the density values.

Table 3. Density values of each specimen.

Specimen	Density (g/cm^3)
PX Cast	1.15 ± 0.007
PX Printed	1.15 ± 0.006
EPL 4 Cast	1.07 ± 0.010
EPL 4 Printed	1.00 ± 0.005

It was found that the PX printed specimen featured a higher density value than the PX cast specimen. This is mainly attributed to the PX printed specimen having residual pentaerythritol whereas the PX cast specimen featured voids. It was determined to be pentaerythritol because it did not react with carbon dioxide and form a white powder when left exposed for 72 hours. Voids developed in the PX cast specimens more than in the PX printed specimens because the PX cast specimens exotherm extensively as they were mixed all at once, and the resulting condensation evaporated. A comparison of each cross section is shown in Figure 13 below taken by the Keyence VHX-7000. The cross section of the PX cast specimen features visible voids whereas the PX printed specimen does not feature voids but possessed some pentaerythritol on the surface. Again it was determined to be pentaerythritol because residual m-xylylenediamine reacts with carbon dioxide and forms a white powder. Voids are marked in Figure 14 with red circles.

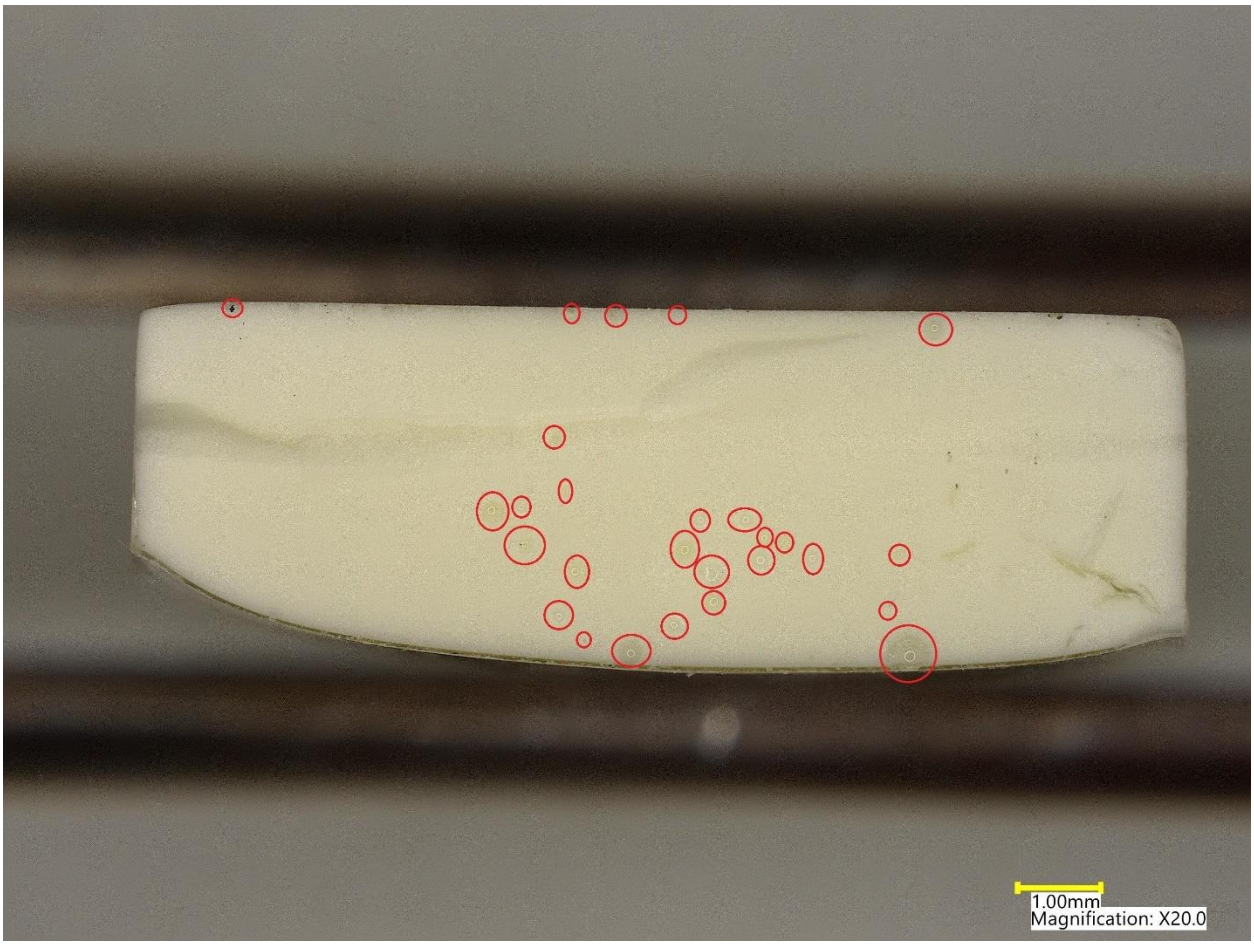

Figure 14. Cross section of PX cast specimen.

6.2. Tensile

Tensile testing was completed for cast and printed versions of the EPL 4 as well as cast, an ideal, and non-ideal version of the PX, all at a crosshead rate of 5 mm/min. All printed specimens were printed with 4 layers. The intent of testing both an ideal version and a non-ideal version of the PX was to illustrate the impact of print resolution in terms of mechanical properties. Different layer heights were used to create the ideal and non-ideal specimens, with non-ideal specimens featuring 2.5 mm height differences after each layer which resulted in excess flow and reduced the print resolution. To achieve a better understanding of what the original G-code path looked like, Figure 15 depicts the print specimens with the G-code path laid on top of the resulting print

specimens. The maximum width of the G-code print path is 18 mm at the width of the tab section and features 2 mm spacing between passes in the whole specimen.

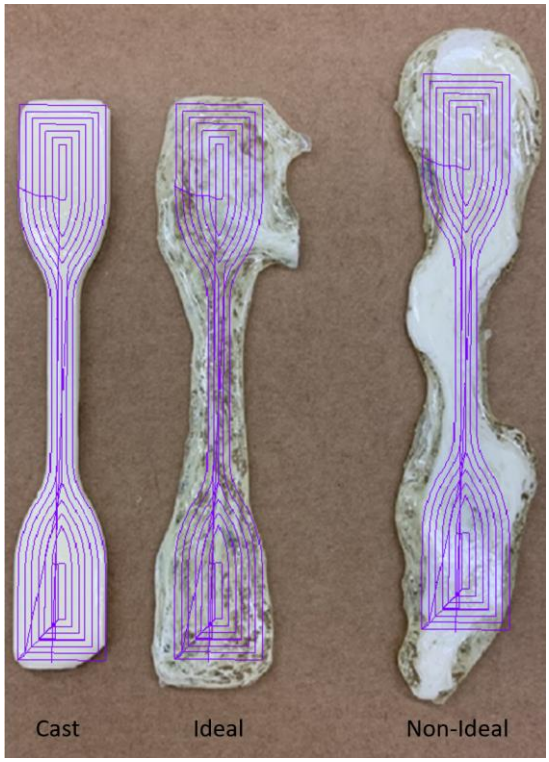

Figure 15. PX printed specimens with highlighted print path imposed on the photo.

The tensile stress confirmed the hypothesis that a lower print resolution contributes to lower mechanical properties. The cross section of non-uniform gauge sections was measured in the smallest area with a caliper and averaged to calculate the tensile stress. The smallest area was assumed to have the highest stress concentration and in turn a higher probability of failing. Specimen failure was observed to have a clean break with little layer to layer debonding. Figure 16 depicts the maximum tensile stress of each type of resin system.

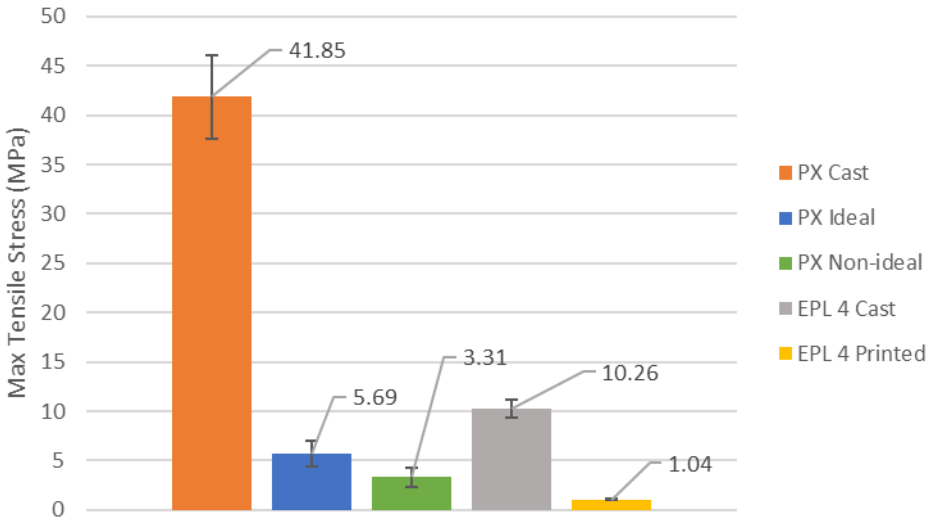

Figure 16. Average maximum tensile strength of PX and EPL 4 specimens.

The EPL 4 cast specimens exhibited the highest strain before failing. In the representative tensile stress versus strain curve below in Figure 17, the EPL 4 cast specimen was required to be stopped early. This is because the representative EPL 4 cast specimen elongated to 149% tensile strain and 10 MPa tensile stress and 149% tensile strain would not fit on the graph.

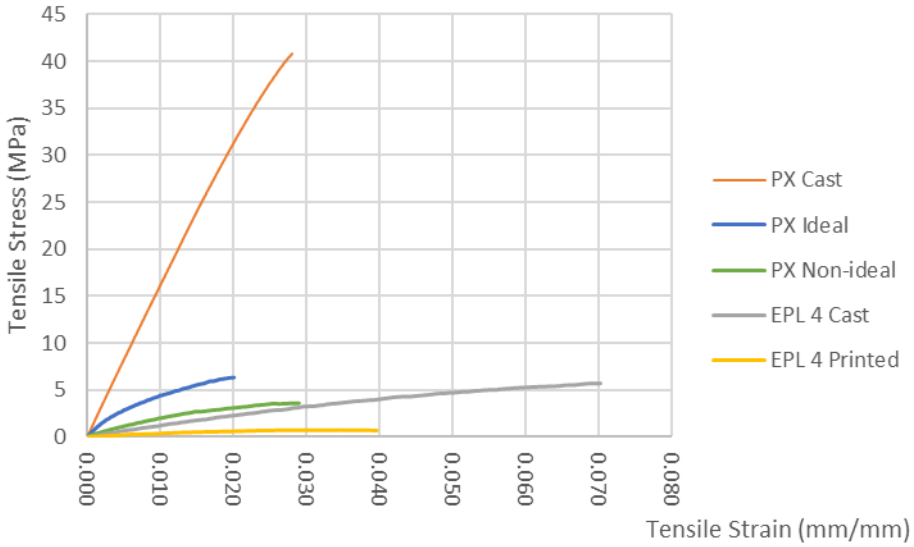

Figure 17. Average maximum tensile strength of PX and EPL 4 specimens.

The PX ideal specimens featured an 86.4% reduction in maximum tensile stress from the PX cast specimens. Whereas the PX non-ideal specimens featured a 92.1% reduction in maximum

tensile stress from the PX cast specimens. The EPL 4 printed specimens showed an 89.9% reduction of maximum tensile stress from the EPL 4 cast specimens. Results for the PX non-ideal specimens have been lower than the PX ideal specimens and a similar trend is shown in Figure 18 which depicts the elastic modulus values of each resin system.

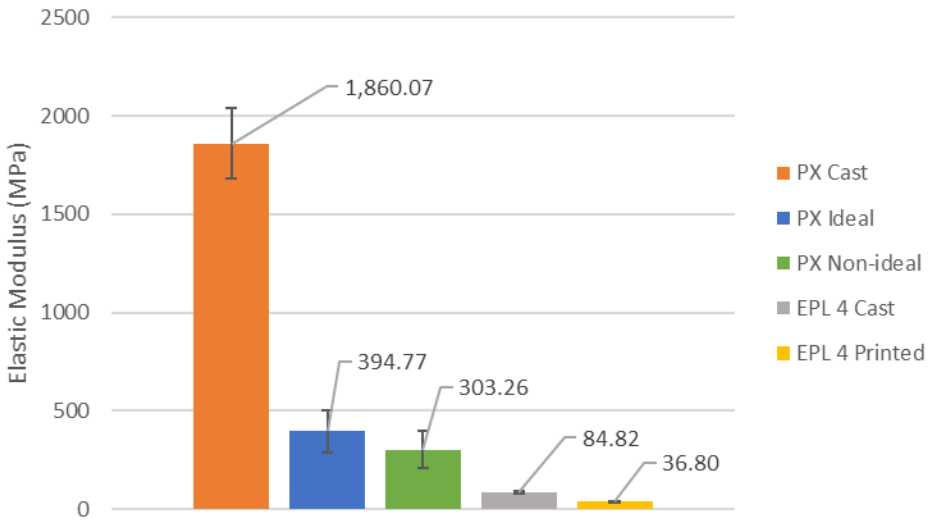

Figure 18. Average elastic modulus values of PX and EPL 4 specimens.

The PX ideal specimens exhibited a 78.8% decrease from the PX cast specimens in elastic modulus, but the PX non-ideal specimens showed an 83.7% decrease in elastic modulus, which reaffirmed the hypothesis. The EPL 4 printed specimens featured a 56.6% reduction in elastic modulus from the EPL 4 cast specimens. Table 4 below depicts a side-by-side comparison of each resin system and the included percent difference for maximum tensile stress and elastic modulus.

Table 4. Tensile test results of each resin system.

Tensile	Stress (MPa)	% Difference	Elastic Modulus (MPa)	% Difference
PX Cast	41.9 ± 4.2	NA	1860.1 ± 181.2	NA
PX Ideal	5.7 ± 1.3	-86.4	394.8 ± 107.9	-78.8
PX Non-ideal	3.3 ± 0.5	-92.1	303.3 ± 96.8	-83.7
EPL 4 Cast	10.3 ± 0.9	NA	84.8 ± 4.7	NA
EPL 4 Printed	1.0 ± 0.1	-89.9	36.8 ± 2.2	-56.6

Given that the PX specimens were more rigid than the EPL 4 specimens, it was expected that the PX specimens would have a lower strain to failure than the EPL 4 specimens. This hypothesis was confirmed during tensile testing as the average strain to failure for the PX cast specimens was 2.5% but the average strain to failure of the EPL 4 cast specimens was 196.0%. Table 5 provides the strain to failure results as well as the percent difference of each resin system. The PX non-ideal specimens featured a 27% drop in strain to failure which was expected as the PX non-ideal specimens featured stress concentrations.

Table 5. Strain to failure.

Strain to Failure	Strain to Fail (%)	% Difference
PX Cast	2.5 ± 0.34	NA
PX Ideal	2.1 ± 0.42	-15.6
PX Non-ideal	1.8 ± 0.56	-27.6
EPL 4 Cast	196.0 ± 28.7	NA
EPL 4 Printed	5.4± 0.1	-97.2

6.3. Flexural

3-point bend flexural testing was completed on both the cast and printed versions of the EPL 4 and the PX. Using Equation 5.2 the crosshead rates for each resin system were determined, EPL 4 cast and printed specimens featured a crosshead rate of 3 mm/min, PX cast specimens utilized a crosshead rate of 1.54 mm/min, and the printed PX specimens featured a crosshead rate of 1.06 mm/min. The maximum flexural stress was taken at 2.6% strain, or failure, as the PX cast specimens failed on average at 2.6% strain. The end of test strain value deviated from the standard to provide better a comparison in the study. Figure 19 features a representative stress versus strain curve of the EPL 4 flexural tests. All printed specimens were printed with 4 layers.

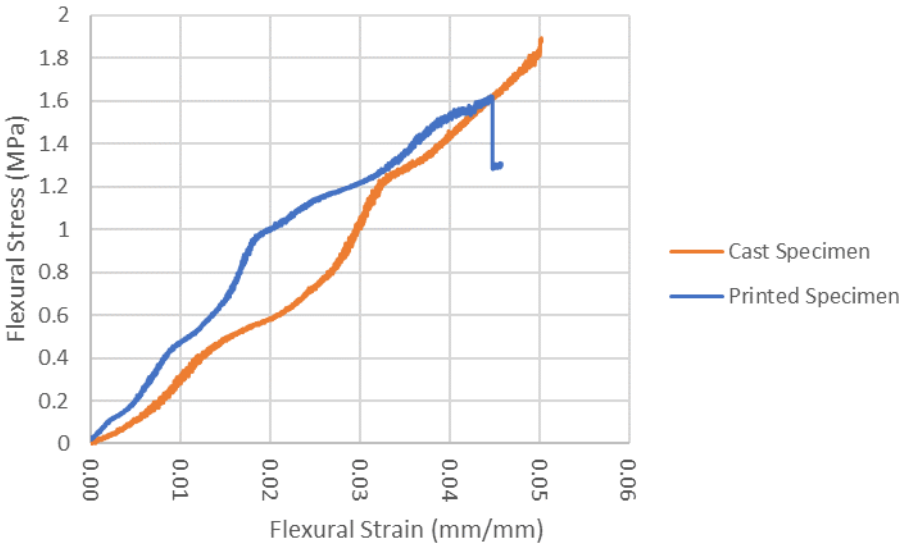

Figure 19. Stress-strain curve of cast and printed EPL 4 specimens.

The lack of linear portions on the curve result from the low load exhibited on the specimen and the use of the 2 kN load cell. The average load required to deflect the cast specimens to 5% strain was 4.0 N. The average load required to deflect the printed specimen to 5% strain was 4.6 N. Figure 20 depicts the stress versus strain curve of a cast and printed PX specimen.

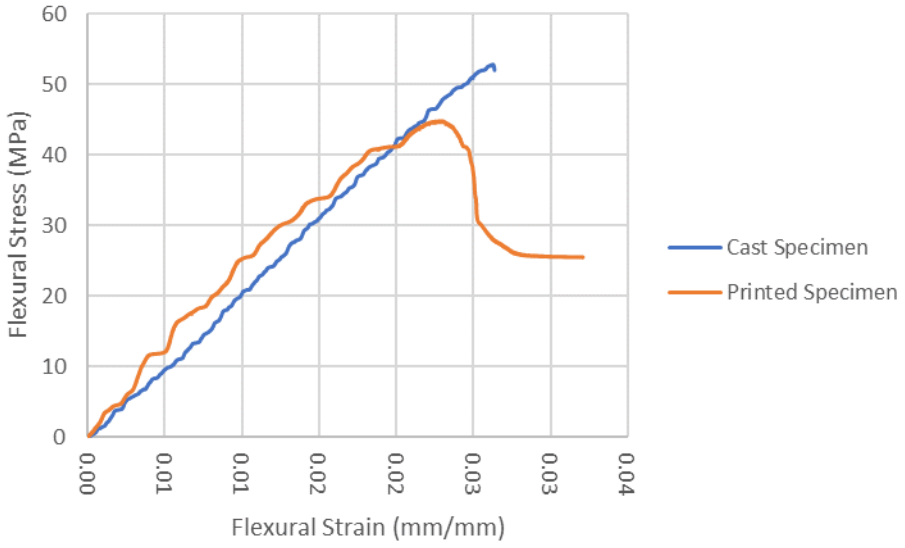

Figure 20. Stress-strain curve of cast and printed PX specimens.

The cast specimen featured linear deformation until failure whereas the printed specimen featured a semi-linear curve that failed before the cast specimen. The average force required for

the cast specimens to fail was 86.20 N and the average force required for the printed specimens to fail was 22.57 N. The noise in each of the stress versus strain curve was a result of the low load on the 2 kN load cell as the 2 kN load cell has an accuracy of 0.5 N [46].

To accurately depict the cross-sectional area of the specimen, a VHS Keyence was used to capture 3D images. The PX printed specimens were partially translucent and partially opaque which results in an inaccurate cross-sectional measurement. To counteract this, a black line was drawn across the specimen which allowed for Keyence to capture an accurate image. Additionally, the Keyence lighting was changed to black and white. Figure 21 below shows the captured image from the Keyence. Figure 22 below depicts a bar graph showing the maximum flexural stress to 2.64% strain including standard deviation bars.

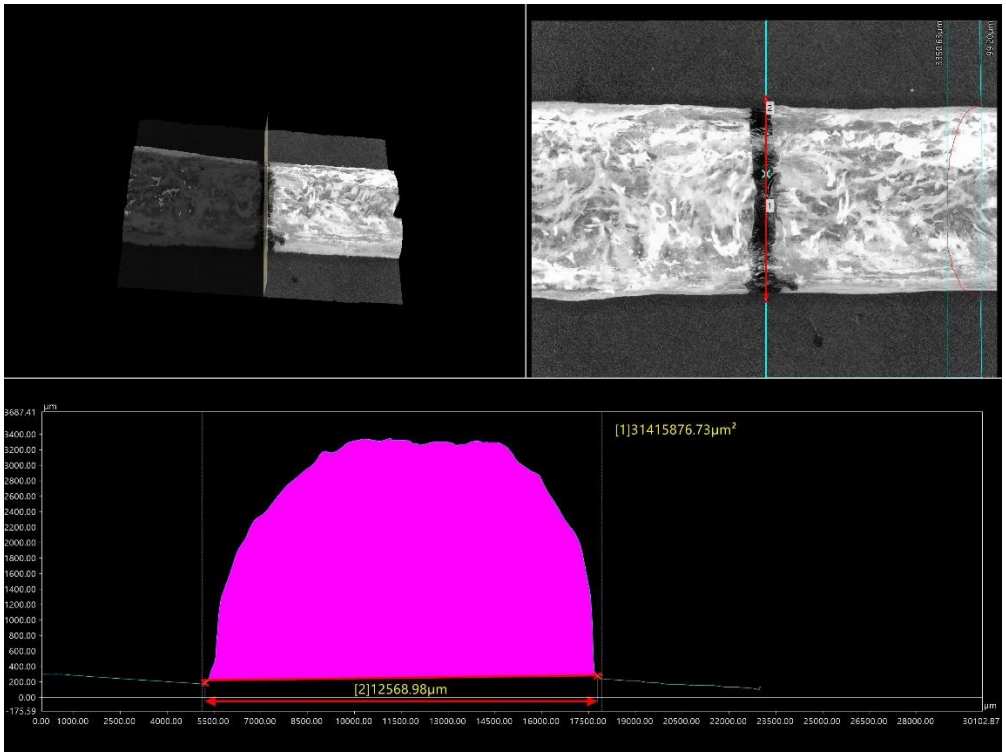

Figure 21. Keyence image of PX printed specimen.

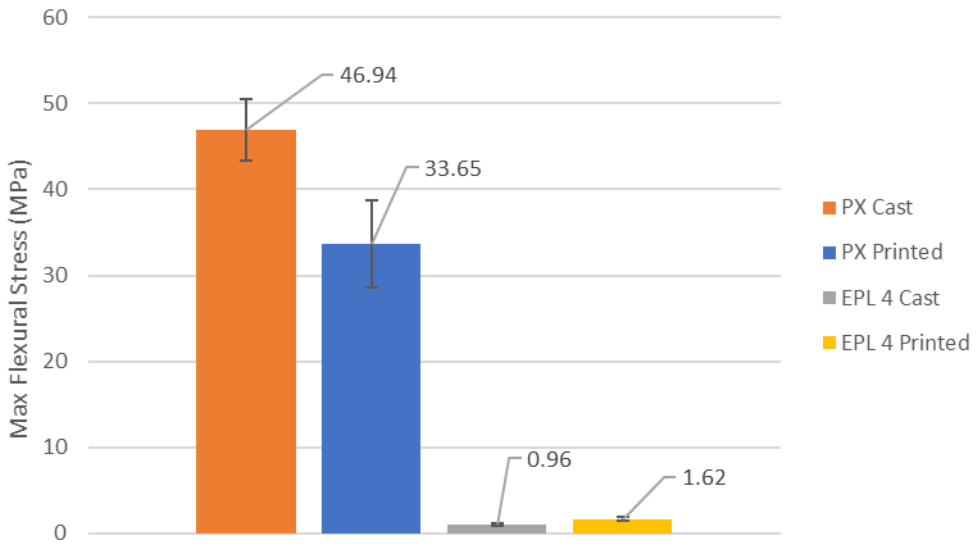

Figure 22. Max flexural stress of PX and EPL 4 specimens.

The increase in flexural properties with the PX resin system was first expected after printing and before testing because the specimens were dry to the touch 2 min after printing and attained a high enough modulus to support itself after it was removed from the bed. In comparison to the EPL 4 which showed signs of excess polyol that remained after printing and was not mixed homogenously. The PX printed specimens exhibited a decrease in flexural strength by 28.31% compared to the PX cast specimens. The EPL 4 printed specimens show an increase of 72.34% of flexural stress at 2.64% strain compared to the EPL 4 cast specimens. This increase was because the EPL 4 cast specimens achieved a higher stress at 5% strain, but all specimens' values were recorded at 2.64% strain. However, the PX printed specimens were not optimally cured, and it was assumed the cast PX specimens were. To illustrate the printed geometry Figure 23 depicts a top-down view of both printed specimens. The EPL 4 flexural specimens had an average width of 20 mm and a length of 120 mm. The PX printed flexural specimens had an average width of 12.5 mm and length of 100 mm.

Figure 23. Top-down view of printed EPL 4 and PX specimens.

Additionally, Figure 24 depicts a photo of a PX printed specimen after deformation from flexural testing. As shown in Figure 24 some excess acetoacetylated pentaerythritol was shown on the tension side of a flexural specimen. It was confirmed to be acetoacetylated pentaerythritol because after 72 h the resulting bead did not react with moisture in the air nor change state. Unreacted m-xylylenediamine was observed to harden and form a white powder within 24 h when exposed to carbon dioxide. Figure 25 shows the flexural modulus results from each resin system with standard deviation bars.

Figure 24. PX flexural specimen leaking pentaerythritol resin.

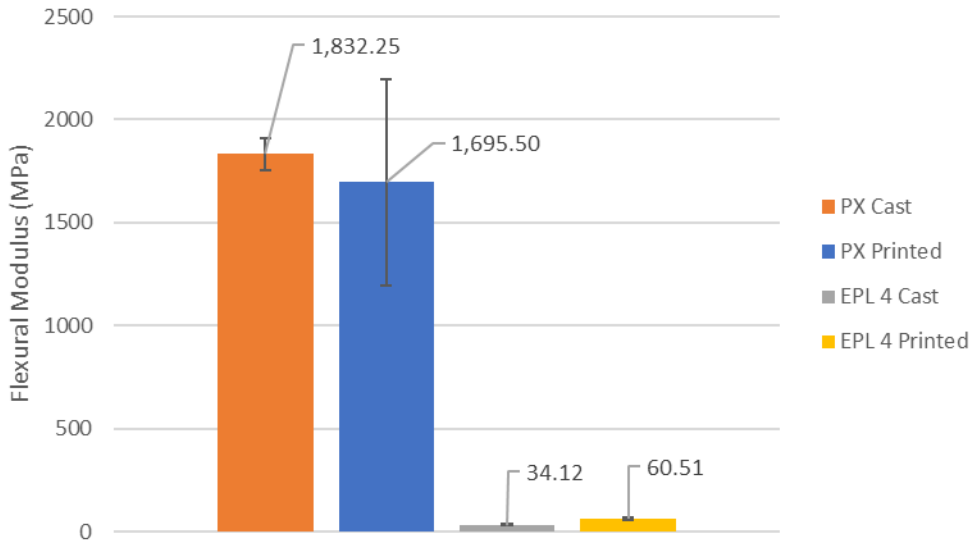

Figure 25. Flexural modulus of PX and EPL 4 specimens.

The flexural modulus of each specimen was taken from 0.01% strain to 1% strain. The flexural modulus of PX printed specimens were 28.3% lower than the PX cast specimen's flexural modulus. EPL 4 printed specimens featured a 77.3% increase in modulus compared to the EPL 4 cast specimens. The increase in properties was because of unreacted isocyanate curing and creating a material with a high modulus [47]. Table 6 below depicts the average flexural stress at 2.6% strain for each specimen and the flexural modulus for each specimen.

Table 6. 3-point bend results of each resin system.

3-Point Bend	Stress at 2.64% (MPa)	% Difference	Flexural Modulus (MPa)	% Difference
PX Cast	46.9 ± 3.6	NA	1832.3 ± 154.3	NA
PX Printed	33.7 ± 8.8	-28.3	1695.5 ± 502.1	-7.5
EPL 4 Cast	0.9 ± 0.1	NA	34.1 ± 4.3	NA
EPL 4 Printed	1.6 ± 0.2	72.3	60.5 ± 6.5	77.3

6.4. Thermogravimetric Analysis

Thermogravimetric analysis of cast and printed EPL 4 and PX specimens was completed and compared. All printed specimens were printed with 4 layers and nitrogen was used to test with. Three specimens of each type were tested, all three sections came from the same specimen but

different locations on the specimen, and the parameters were temperature ramp of 10 °C per minute, starting at 20 °C and finishing at 600 °C. The printed specimen sizes ranged from 13.5 mg to 45.4 mg. The two materials have vastly different properties as shown in the tensile and flexural testing sections. It was expected that the printed specimens would have a lower degradation temperature as the printed specimens were not fully cured and would then start to degrade sooner due to having less cross-linking within the polymer chains. A representative TGA graph is exhibited in Figure 26.

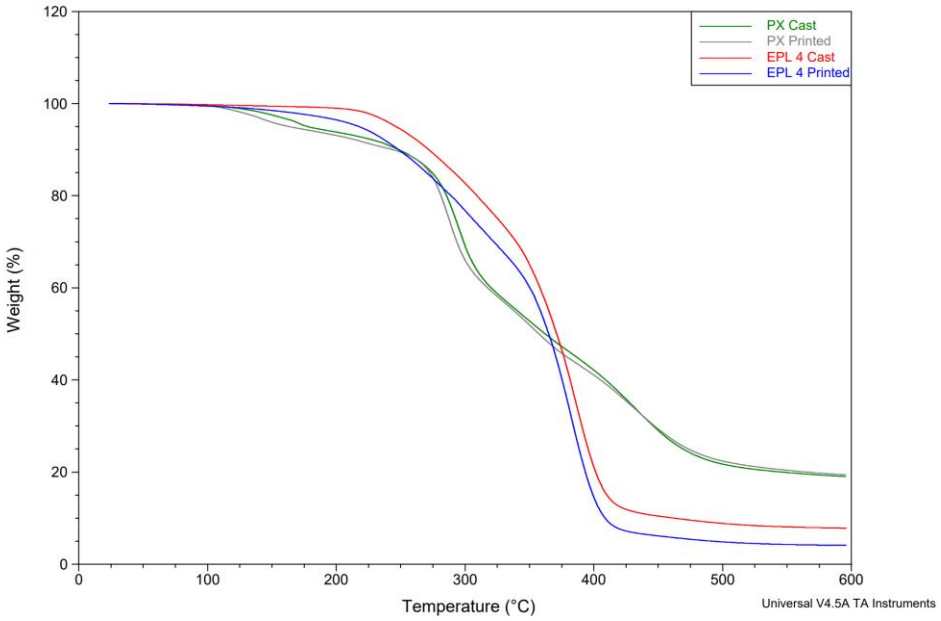

Figure 26. Representative TGA curve of each specimen.

Table 7 depicts the degradation temperature for each of the specimens. The EPL 4 printed specimens degraded from 125 °C to 175 °C and the EPL 4 cast specimens showed initial degradation from 175 °C to 200 °C. The PX printed specimens showed initial mass loss 85 °C to 100 °C and the cast specimens showed an initial mass loss from 100 °C to 115 °C. The initial mass loss at lower temperatures indicated the vaporization of unmixed reactive resin in both systems.

Table 7. Degradation temperature of EPL 4 and PX specimens.

Specimen Type	EPL 4 (°C)	% Difference	PX (°C)	% Difference
Cast	324.6 ± 3.6	NA	261.2 ± 1.2	NA
Printed	321.2 ± 1.5	-1.1	256.3 ± 1.4	-1.9

6.5. Differential Scanning Calorimetry

The glass transition temperature is the temperature where a polymer changes from a glass state to a rubber state. Given that the EPL 4 is an elastomeric material, rubbery at room temperature, it was expected to have a glass transition temperature below 0 °C. The PX specimens were rigid at room temperature and were expected to have a glass transition temperature above 20 °C. Each printed specimen was expected to have a lower glass transition temperature and it was proved in the results. Below in Figure 27 is a representative DSC graph. All printed specimens were printed with 4 layers.

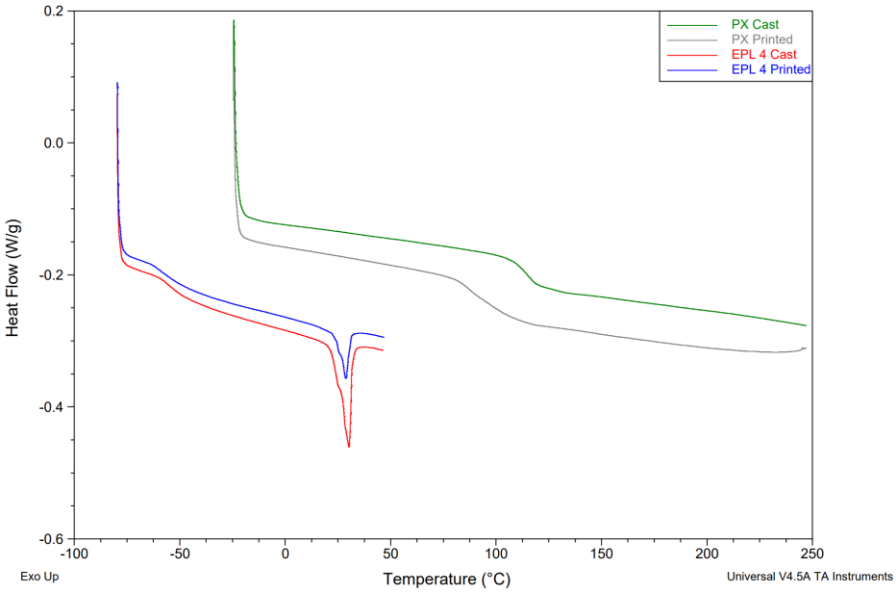

Figure 27. Representative DSC curve of each specimen.

The reason printed specimens exhibited a lower glass transition temperature was because the printed specimens received a lower quality mix than their respective cast specimens. With a

lower quality mix the polymer chains are not fully cross-linked and require a lower temperature to bring the polymer chains out of the free state. The endothermic peaks that are observed for the EPL 4 specimens near room temperature is the crystalline phase melting [48]. Table 8 depicts the glass transition temperature values for both the cast and printed versions of EPL 4 and PX.

Table 8. Glass transition temperature of EPL 4 and PX specimens.

Specimen Type	EPL 4 (°C)	% Difference	PX (°C)	% Difference
Cast	-55.0 ± 0.6	NA	115.6 ± 1.6	NA
Printed	-57.7 ± 1.1	-4.96	91.4 ± 1.8	-20.9

7. CONCLUSION AND FUTURE RECOMMENDATIONS

7.1. Conclusion

To summarize, Section 6 showcased that the PX specimens achieved higher mechanical properties than the EPL 4 specimens. Given that the PX specimens were tailored to be printed and the EPL 4 resin was a commercial resin intended for hand mixing, the PX resin system showcased more ideal process parameters. Given that the materials are two very different types, EPL 4 was more elastomeric than the PX, comparisons were drawn from cast specimens versus printed specimens of the same resin system.

The printed specimens featured a drop in properties aside from the EPL 4 flexural specimens which was because the stress values were taken at 2.6% strain instead of 5%. The EPL 4 printed specimens also featured an increase in flexural modulus by 77.3% over the EPL 4 cast specimen because of the unlinked isocyanate. The PX printed specimens featured a 28.3% decrease in flexural stress from the PX cast specimens but only a 7.5% loss in flexural modulus.

PX specimens were printed with varying print resolutions to test the effect of print resolution on mechanical properties. With low print resolution specimens obtained significantly more stress concentration points that lead to early failure. The PX non-ideal specimens featured a decrease 27.6% in maximum tensile strength compared to the PX cast specimens where the PX ideal specimens only featured a 15.6% decrease in maximum tensile strength. The PX printed specimens showed less of a decrease in mechanical properties than the EPL 4 printed specimens. It is concluded that the PX resin system is a superior resin system for the objectives because of the increase in mechanical properties combined with ideal process parameters. Reactive extrusion additive manufacturing is an emerging industry and will have many applications in the future.

7.2. Future Recommendations

The findings from this study can be extended and optimized in the future. Other two-part reactive resin systems can be used with the printer developed and proven. Additional resin system utilization would show the versatility of the printer as well as warrant more data for a journal article. Continuous carbon fiber introduction was completed but the print parameters were not optimized. Optimization of print parameters as well as use of any continuous fiber would also provide more data for future journal articles. A change in resin system from the PX resin system could allow the fiber to stay in place and help optimize print parameters. Figure 28 shows the unoptimized continuous carbon fiber print.

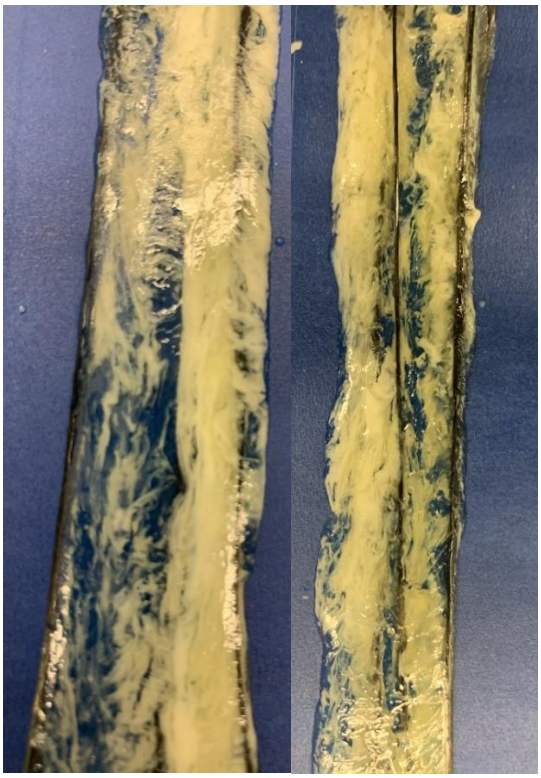

Figure 28. PX specimen with continuous carbon fiber.

To help keep the carbon fiber in place a z-reinforced bed could be utilized. An invention disclosure to North Dakota State University has been made to protect this idea. In addition to holding carbon fiber in place it can also be composed of natural fibers to create a hybrid composite.

Additionally, the z-reinforcement can act as support structure and would eliminate the need to print support structure in the future. Printing with the PX resin as well as printing with the continuous carbon fiber into the Z-reinforced bed has been completed but print parameters need optimization. Figure 29 depicts a photo of a z-reinforced bed which is composed of Tampico fibers and the base made of EPL 4 resin.

Figure 29. Z-reinforced bed of Tampico fibers.

With uniform z-fiber spacing, it can be possible to change fiber layup direction each layer. Figure 30 below depicts a z-reinforced uniformly spaced bed with carbon fiber. To change fiber layup direction the print head can weave around the z fibers and result in a 45° and 90° fiber orientation. Additional print parameter optimization needs to occur as well as optimizing the matrix system.

Figure 30. Uniform z fiber reinforced bed with continuous carbon fiber printed on top.

Introduction of a continuous fiber to a liquid reaction resin system proved to be difficult initially. To introduce a continuous fiber the area must be low pressure, so the resin does not flow through the fiber inlet hole and instead can flow through nozzle exit. Below, Figure 31, depicts the proposed solution of introducing a fiber in a low-pressure environment.

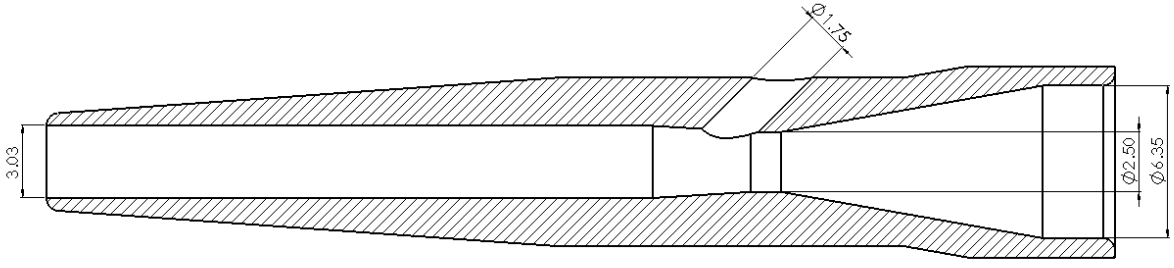

Figure 31. Section view of venturi nozzle.

The venturi effect is the phenomena that results when pressure decreases and velocity increases [48]. This effect can be observed when a fluid flow is constricted through a section of

pipe. A schematic of the required dimensions of a pipe to undergo the venturi effect is depicted below in Figure 32. This diagram was used to calculate the dimensions needed to create a low-pressure environment to introduce the fiber. A prototype was created using Solidworks 2018 (Waltham, Massachusetts) and was created with the Form 2 with 25 μm print resolution.

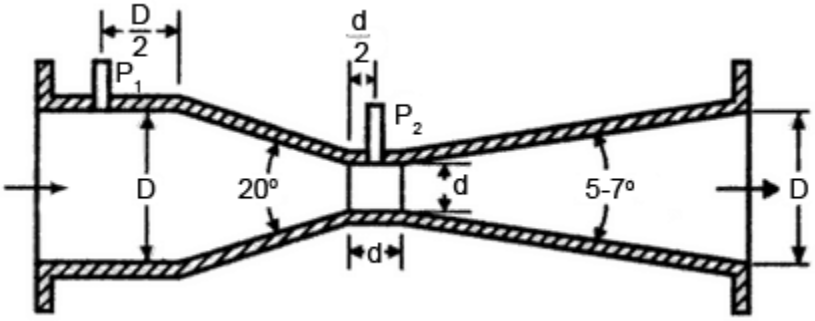

Figure 32. Venturi effect pipe dimensions [49].

The next step is to refine the print parameters to decrease the excess resin. The excess resin exhibited in Figure 30, is the result of decreasing the feed rate and maintaining the flow rate. After print parameter refinement, mechanical testing and large-scale printing can be completed. To showcase the effect of z reinforcement, compression testing should be completed. Finally, a journal article should be created to illustrate the findings.

REFERENCES

[1] D. L. Bourell, J. J. Beaman, and T. Wohlers, “History and Evolution of Additive Manufacturing,” *Additive Manufacturing Processes*, pp. 11–18, Mar. 2020, doi: 10.31399/ASM.HB.V24.A0006548.

[2] X. Wang, M. Jiang, Z. Zhou, J. Gou, and D. Hui, “3D printing of polymer matrix composites: A review and prospective,” *Composites Part B: Engineering*, vol. 110, pp. 442–458, Feb. 2017, doi: 10.1016/J.COMPOSITESB.2016.11.034.

[3] J. P. Kruth, G. Levy, F. Klocke, and T. H. C. Childs, “Consolidation phenomena in laser and powder-bed based layered manufacturing,” *CIRP Annals*, vol. 56, no. 2, pp. 730–759, Jan. 2007, doi: 10.1016/J.CIRP.2007.10.004.

[4] K. v. Wong and A. Hernandez, “A Review of Additive Manufacturing,” *ISRN Mechanical Engineering*, vol. 2012, pp. 1–10, Aug. 2012, doi: 10.5402/2012/208760.

[5] J. v. Crivello and E. Reichmanis, “Photopolymer Materials and Processes for Advanced Technologies,” *Chemistry of Materials*, vol. 26, no. 1, pp. 533–548, Jan. 2013, doi: 10.1021/CM402262G.

[6] C. W. Hull, “Method for production of three-dimensional objects by stereolithography,” Apr. 1989.

[7] E. J. Murphy, D. Plaines, R. E. Ansel, H. Estates, and J. J. Krajewski, “Investment casting utilizing patterns produced by stereolithography,” Aug. 1988.

[8] I. Gibson, D. Rosen, B. Stucker, and M. Khorasani, “Design for Additive Manufacturing,” *Additive Manufacturing Technologies*, pp. 555–607, 2021, doi: 10.1007/978-3-030-56127-7_19.

[9] J.-P. Fouassier and J. F. RABEK, “Radiation Curing in Polymer Science and Technology: Practical aspects and applications,” p. 542, 1993, Accessed: Jul. 16, 2021. [Online]. Available: https://books.google.co.th/books?id=NQCwBFmr90gC

[10] L. Lu, J. Y. H. Fuh, A. Y. C. Nee, E. T. Kang, T. Miyazawa, and C. M. Cheah, “Origin of shrinkage, distortion and fracture of photopolymerized material,” *Materials Research Bulletin*, vol. 30, no. 12, pp. 1561–1569, Dec. 1995, doi: 10.1016/0025-5408(95)00118-2.

[11] J. K. Fink, “Reactive Polymers Fundamentals and Applications: A Concise Guide to Industrial Polymers: Second Edition,” *Reactive Polymers Fundamentals and Applications: A Concise Guide to Industrial Polymers: Second Edition*, pp. 1–535, 2013, doi: 10.1016/C2012-0-02516-1.

[12] L. Y. Lin, J. H. Lee, C. E. Hong, G. H. Yoo, and S. G. Advani, “Preparation and characterization of layered silicate/glass fiber/epoxy hybrid nanocomposites via vacuum-assisted resin transfer molding (VARTM),” *Composites Science and Technology*, vol. 66, no. 13, pp. 2116–2125, Oct. 2006, doi: 10.1016/J.COMPSCITECH.2005.12.025.

[13] F. L. Jin, X. Li, and S. J. Park, “Synthesis and application of epoxy resins: A review,” *Journal of Industrial and Engineering Chemistry*, vol. 29, pp. 1–11, Sep. 2015, doi: 10.1016/J.JIEC.2015.03.026.

[14] O. Uitz, P. Koirala, M. Tehrani, and C. C. Seepersad, “Fast, low-energy additive manufacturing of isotropic parts via reactive extrusion,” *Additive Manufacturing*, vol. 41, p. 101919, May 2021, doi: 10.1016/J.ADDMA.2021.101919.

[15] C. C. Ibeh, “Phenol-Formaldehyde Resins,” *Handbook of Thermoset Plastics*, pp. 23–71, Jan. 1998, doi: 10.1016/B978-081551421-3.50005-9.

[16] a. B. Strong, “Plastics: Materials and Processing,” *Science and Technology of Advanced Materials*, vol. 14, p. 917, 2006, Accessed: Jul. 13, 2021. [Online]. Available: http://books.google.com/books/about/Plastics.html?id=NdJRAAAAMAAJ&pgis=1

[17] L. Z. Linganiso and R. D. Anandjiwala, “Fibre-reinforced laminates in aerospace engineering,” *Advanced Composite Materials for Aerospace Engineering*, pp. 101–127, Jan. 2016, doi: 10.1016/B978-0-08-100037-3.00004-3.

[18] D. Dimesko, G. Bogoevea-Gaceva, and V. Srebrenkoska, “Resin content and molding pressure influence on ballistic properties and trauma effect of aromatic amide fibers composites - UGD Academic Repository,” 2011. https://eprints.ugd.edu.mk/2731/ (accessed Jul. 13, 2021).

[19] H. J. Fabris and W. G. Knauss, “Synthetic Polymer Adhesives,” *Comprehensive Polymer Science and Supplements*, pp. 131–177, Jan. 1989, doi: 10.1016/B978-0-08-096701-1.00208-1.

[20] G. Marsh, “Fire-safe composites for mass transit vehicles,” *Reinforced Plastics*, vol. 46, no. 9, pp. 26–30, Sep. 2002, doi: 10.1016/S0034-3617(02)80157-6.

[21] H. Masuda, Y. Ohta, and M. Kitayama, “Additive Manufacturing of SiC Ceramics with Complicated Shapes Using the FDM Type 3D-Printer,” *Journal of Materials Science and Chemical Engineering*, vol. 07, no. 02, pp. 1–12, Feb. 2019, doi: 10.4236/MSCE.2019.72001.

[22] Z. S. Petrović and J. Ferguson, “Polyurethane elastomers,” *Progress in Polymer Science*, vol. 16, no. 5, pp. 695–836, 1991, doi: 10.1016/0079-6700(91)90011-9.

[23] “SELF LEVELING POLYUREA ELASTOMER”, Accessed: Aug. 01, 2021. [Online]. Available: www.specialty-products.com.

[24] “POLYSHIELD HT ™ 100F UB”, Accessed: Aug. 01, 2021. [Online]. Available: www.specialty-products.com.

[25] D. Kokkinis, M. Schaffner, and A. R. Studart, “Multimaterial magnetically assisted 3D printing of composite materials,” *Nature Communications 2015 6:1*, vol. 6, no. 1, pp. 1–10, Oct. 2015, doi: 10.1038/ncomms9643.

[26] Chris. Rauwendaal, “Mixing in polymer processing,” p. 475, 1991.

[27] Ganapathy Subramanian and Santhana Gopinath, “A CONTINUOUS IMPINGEMENT MIXING PROCESS FOR EFFECTIVE DISPERSION OF NANOPARTICLES IN POLYMERS,” 2006.

[28] M. K. Singh, T. G. Kang, P. D. Anderson, H. E. H. Meijer, and A. N. Hrymak, “Analysis and optimization of low-pressure drop static mixers,” *AIChE Journal*, vol. 55, no. 9, pp. 2208–2216, Sep. 2009, doi: 10.1002/AIC.11846.

[29] R. K. Thakur, C. Vial, K. D. P. Nigam, E. B. Nauman, and G. Djelveh, “Static Mixers in the Process Industries—A Review,” *Chemical Engineering Research and Design*, vol. 81, no. 7, pp. 787–826, Aug. 2003, doi: 10.1205/026387603322302968.

[30] O. Rios *et al.*, “3D printing via ambient reactive extrusion,” *Materials Today Communications*, vol. 15, pp. 333–336, Jun. 2018, doi: 10.1016/J.MTCOMM.2018.02.031.

[31] “Volumetric dosing technology by ViscoTec - for viscous materials.” https://www.viscotec.de/en/technology/ (accessed Jul. 20, 2021).

[32] P. Fisch, M. Holub, and M. Zenobi-Wong, “Improved accuracy and precision of bioprinting through progressive cavity pump-controlled extrusion,” *Biofabrication*, vol. 13, no. 1, p. 015012, Dec. 2020, doi: 10.1088/1758-5090/ABC39B.

[33] D. Kokkinis, F. Bouville, and A. R. Studart, “3D Printing of Materials with Tunable Failure via Bioinspired Mechanical Gradients,” *Advanced Materials*, vol. 30, no. 19, p. 1705808, May 2018, doi: 10.1002/ADMA.201705808.

[34] F. Bos, R. Wolfs, Z. Ahmed, and T. Salet, “Additive manufacturing of concrete in construction: potentials and challenges of 3D concrete printing,” *https://doi.org/10.1080/17452759.2016.1209867*, vol. 11, no. 3, pp. 209–225, Jul. 2016, doi: 10.1080/17452759.2016.1209867.

[35] C. BG and L. JA, “3D-printing of lightweight cellular composites,” *Advanced materials (Deerfield Beach, Fla.)*, vol. 26, no. 34, pp. 5930–5935, Sep. 2014, doi: 10.1002/ADMA.201401804.

[36] “EPL™ 4 - Specialty Products, Inc.” http://specialty-products.com/spi_products/epl-4/ (accessed Jul. 13, 2021).

[37] G. Cook, “Enamines : Synthesis: Structure, and Reactions, Second Edition.”, Accessed: Jul. 20, 2021. [Online]. Available: https://books.google.com/books/about/Enamines.html?id=ilQPEAAAQBAJ

[38] “Static Mixer Designs and Applications”.

[39] H. E. H. Meijer, M. K. Singh, and P. D. Anderson, “On the performance of static mixers: A quantitative comparison,” *Progress in Polymer Science*, vol. 37, no. 10, pp. 1333–1349, Oct. 2012, doi: 10.1016/J.PROGPOLYMSCI.2011.12.004.

[40] “G & M Code REFERENCE MANUAL Specializing in CNC Automation and Motion Control,” 2016, Accessed: Aug. 03, 2021. [Online]. Available: www.MachMotion.com

[41] “Instron 2525 Series Drop-through - Instron.” https://www.instron.com/en-us/products/testing-accessories/load-cells/static/2525-series-drop-through (accessed Aug. 21, 2021).

[42] N. Wingborg, “Increasing the tensile strength of HTPB with different isocyanates and chain extenders,” *Polymer Testing*, vol. 21, no. 3, pp. 283–287, Jan. 2002, doi: 10.1016/S0142-9418(01)00083-6.

[43] S. Das *et al.*, “Structure–property relationships and melt rheology of segmented, non-chain extended polyureas: Effect of soft segment molecular weight,” *Polymer*, vol. 48, no. 1, pp. 290–301, Jan. 2007, doi: 10.1016/J.POLYMER.2006.10.029.

APPENDIX

Table A1. Attempted resin systems before EPL 4 and PX.

Commercial or custom	Part 1	Part 2
Specialty Products (Commercial)	Polyshield HT 100F A	Polyshield HT 100 F B
Custom 1	30% Glycerol & 70% Sucrose	DETA 1768 2:1
Custom 2	30% Glycerol & 70% Sucrose	DYTEKA 1768 1:3
Custom 3	30% Glycerol & 70% Sucrose	DYTREKA 1769
Custom 4	30% Glycerol & 70% Sucrose	Ancamine 1769
Custom 5	30% Glycerol & 70% Sucrose	Ancamine 2071
Custom 6	30% Glycerol & 70% Sucrose	DYTEKA Ancamine 2071 1:3
Custom 7	30% Glycerol & 70% Sucrose	DYTEKA Ancamine 2071 1:3 & 2% TEA
Custom 8	30% Glycerol & 70% Sucrose	2% Guiacol DYTEKA 2071
Custom 9	50 % Glycerol & 50% Sucrose	DYTEKA 2071
Custom 10	70% Glycerol & 30% Sucrose	2009 HSF DYTEKA 1:3
Custom 11	70% Glycerol & 30% Sucrose	2007 5% TEA
Custom 12	70% Glycerol & 30% Sucrose	2007 DYTEKA 1:3
Custom 13	70% Glycerol & 30% Sucrose & 2% Guiacol	DYTEKA Ancamine 2071 1:3
Custom 14	70% Glycerol & 30% Sucrose & 2% Guiacol	DYTEKA Ancamine 2071 1:3 2% TEA
Custom 15	AH-10K Pentaerythritol	DYTEKA Ancamine 1:3
Custom 16	AH-10K Pentaerythritol	2007 5% TEA
Custom 17	AH-10K Pentaerythritol	3-Cyclohexanebis(methylamine)
Custom 18	AH-10K Pentaerythritol	Furandiamine

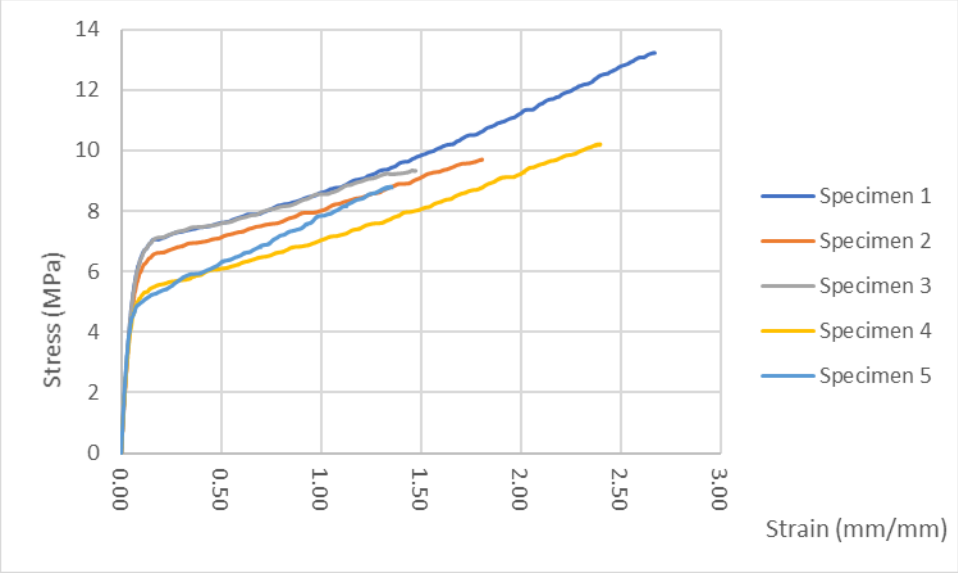

Figure A1. EPL 4 cast tensile results.

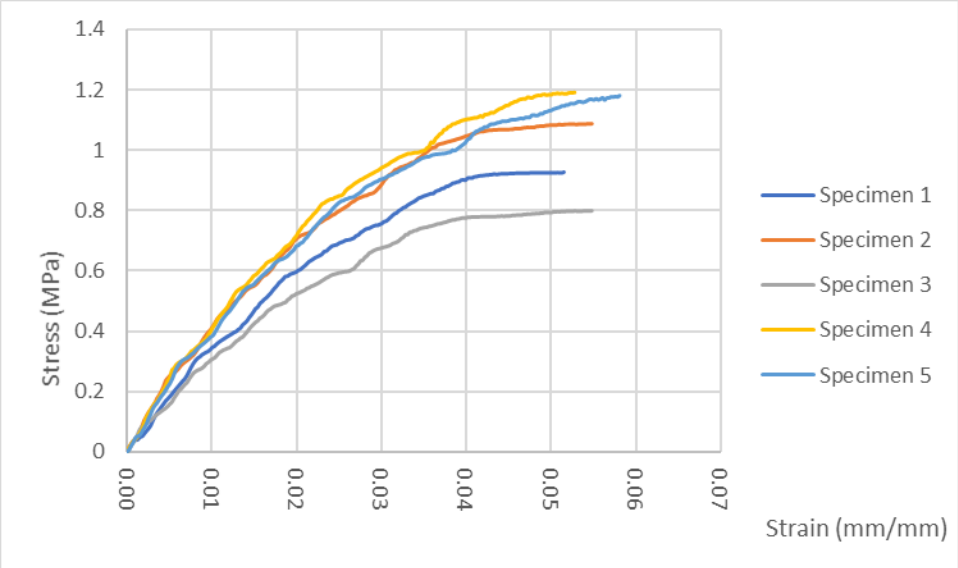

Figure A2. EPL 4 printed tensile results.

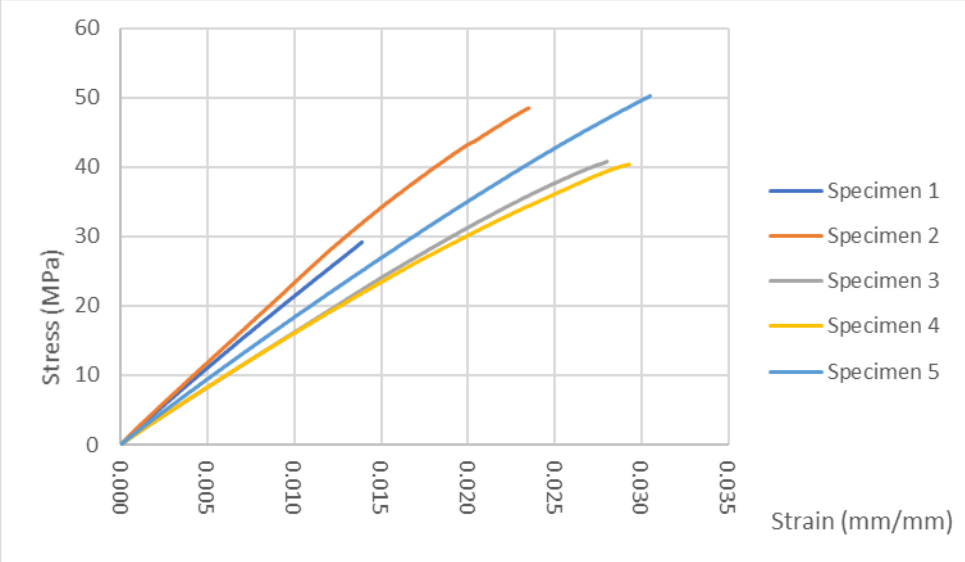

Figure A3. PX cast tensile results.

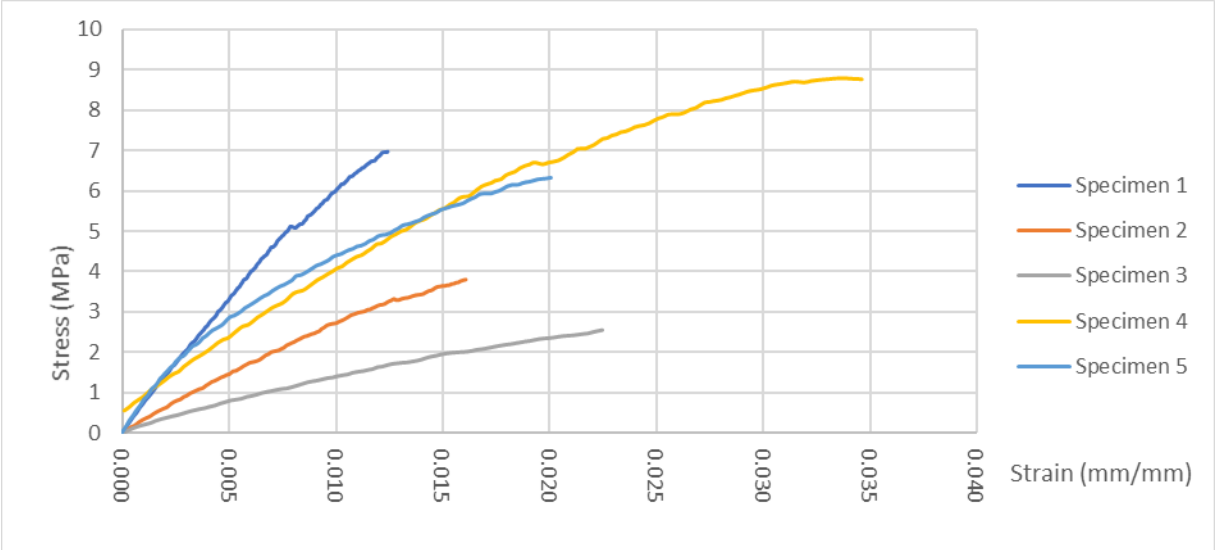

Figure A4. PX ideal tensile results.

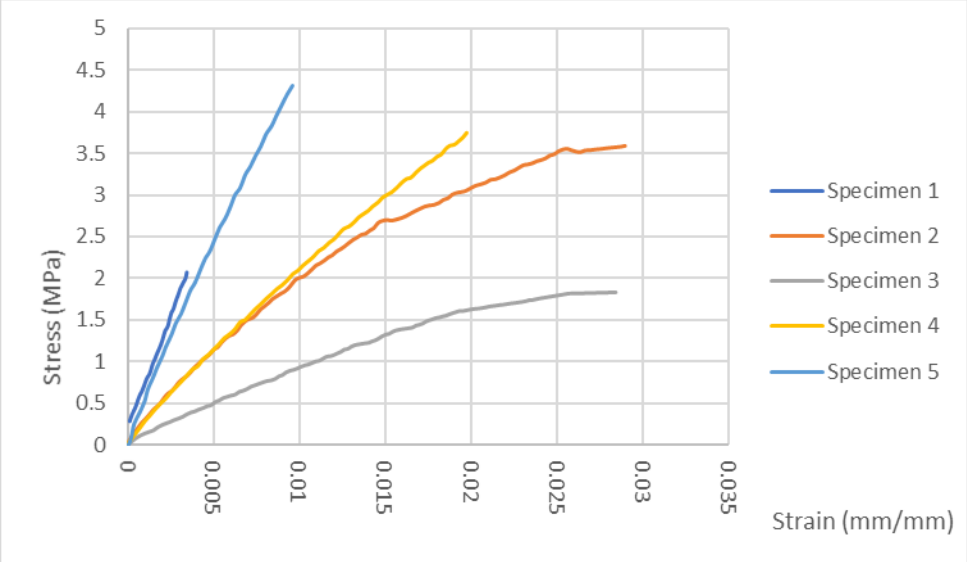

Figure A5. PX non-ideal tensile results.

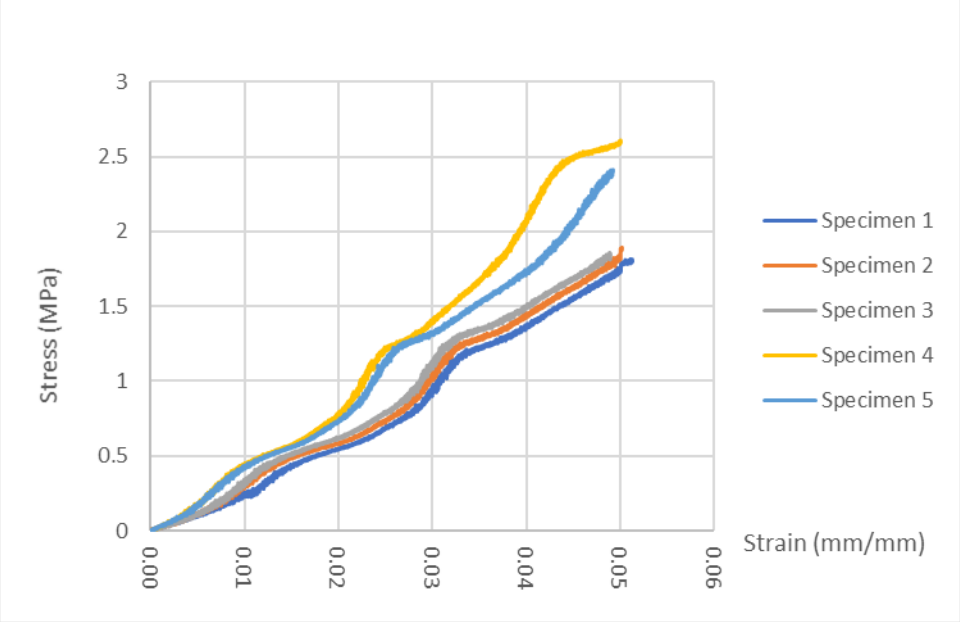

Figure A6. EPL 4 cast flexural results.

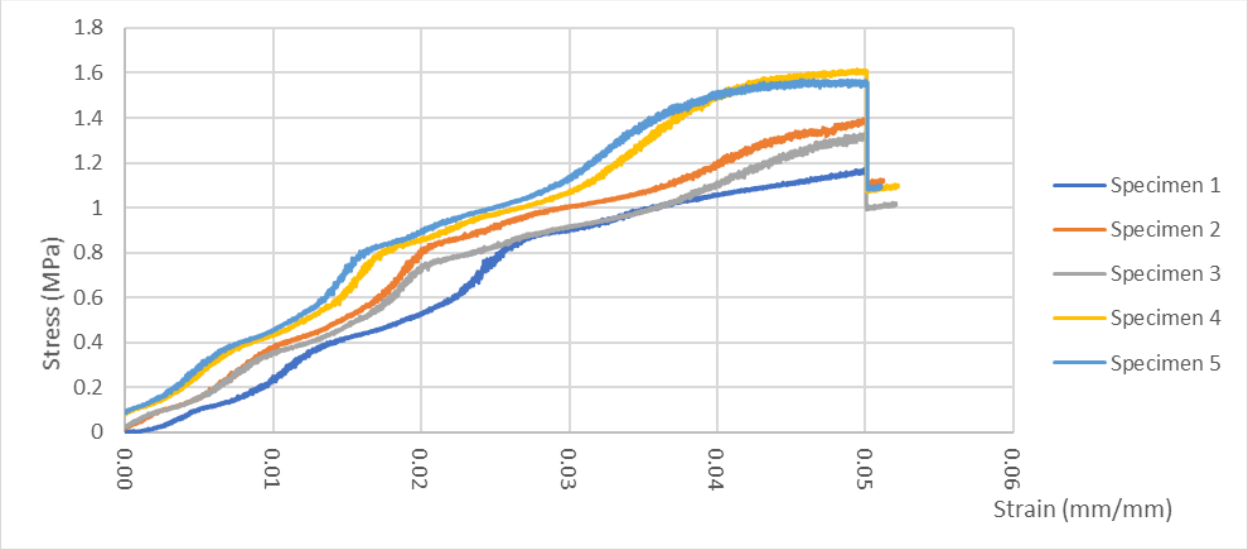

Figure A7. EPL 4 printed flexural results.

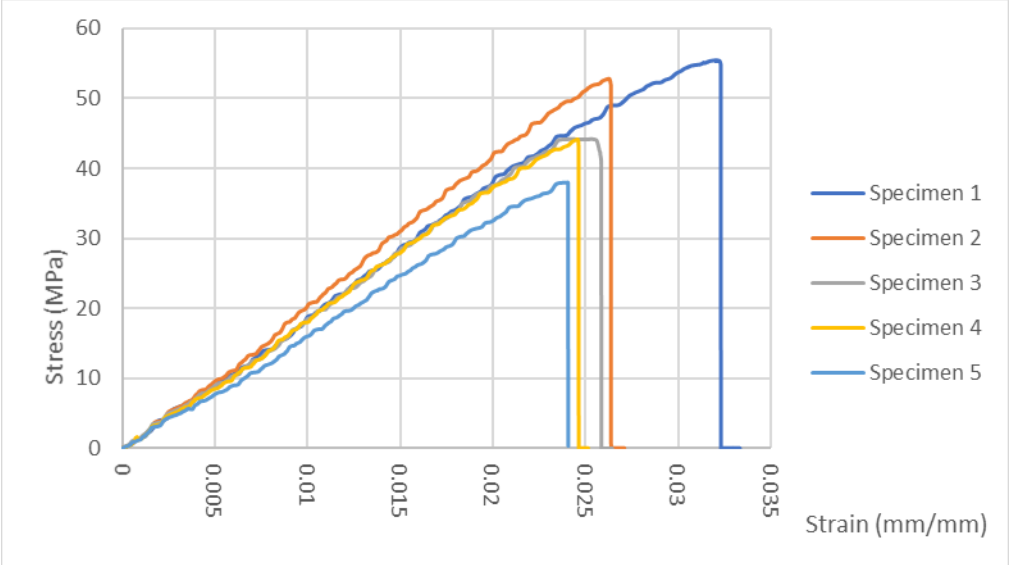

Figure A8. PX cast flexural results.

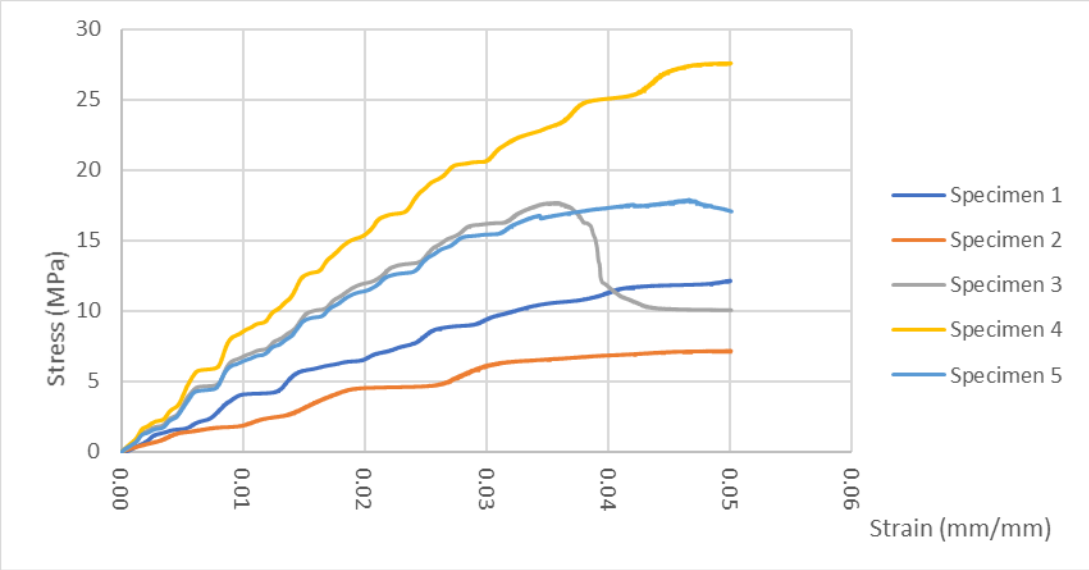

Figure A9. PX printed flexural results.

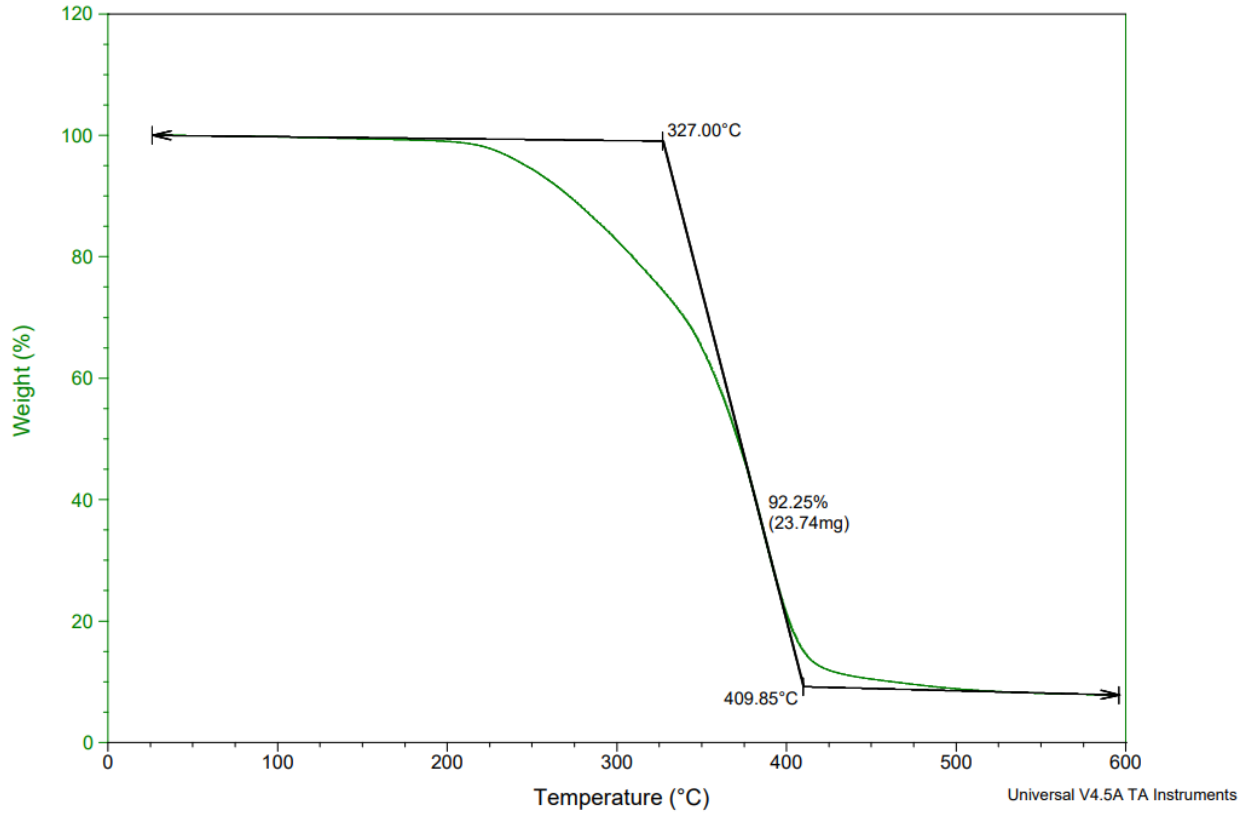

Figure A10. EPL 4 cast specimen 1 TGA results.

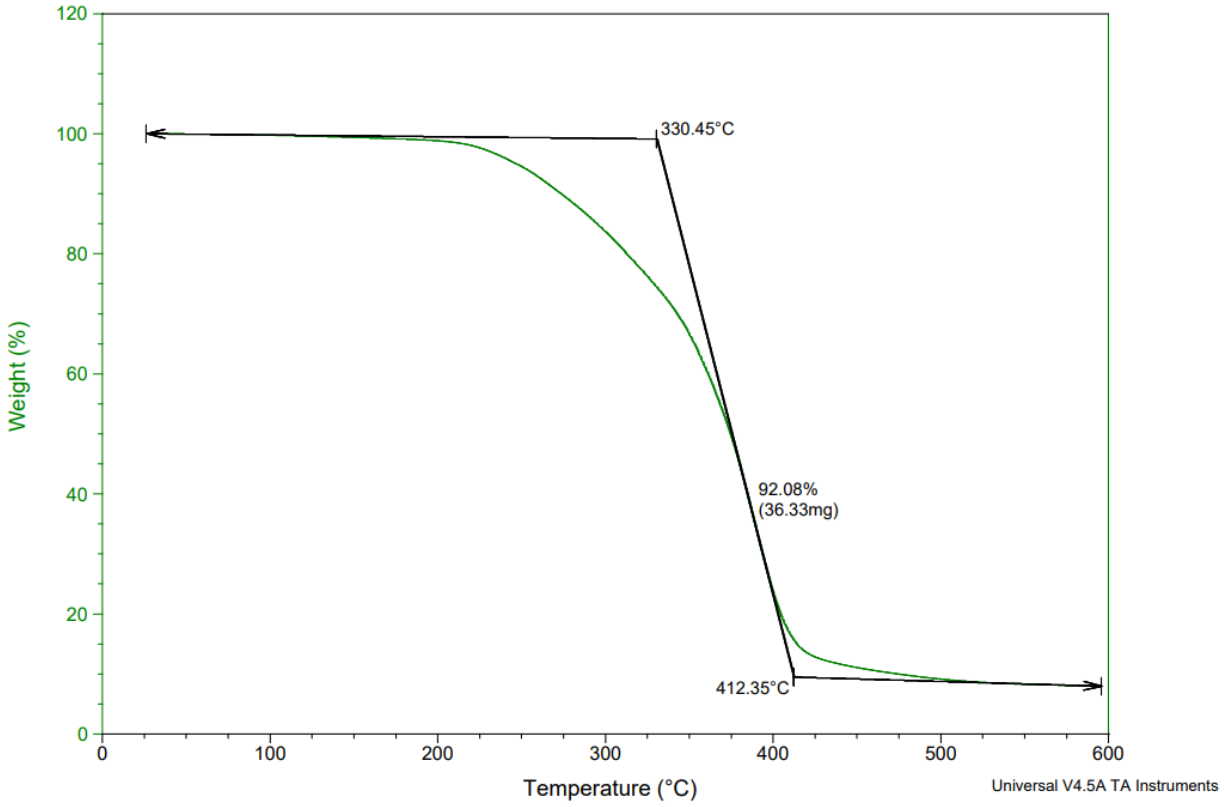

Figure A11. EPL 4 cast specimen 2 TGA results.

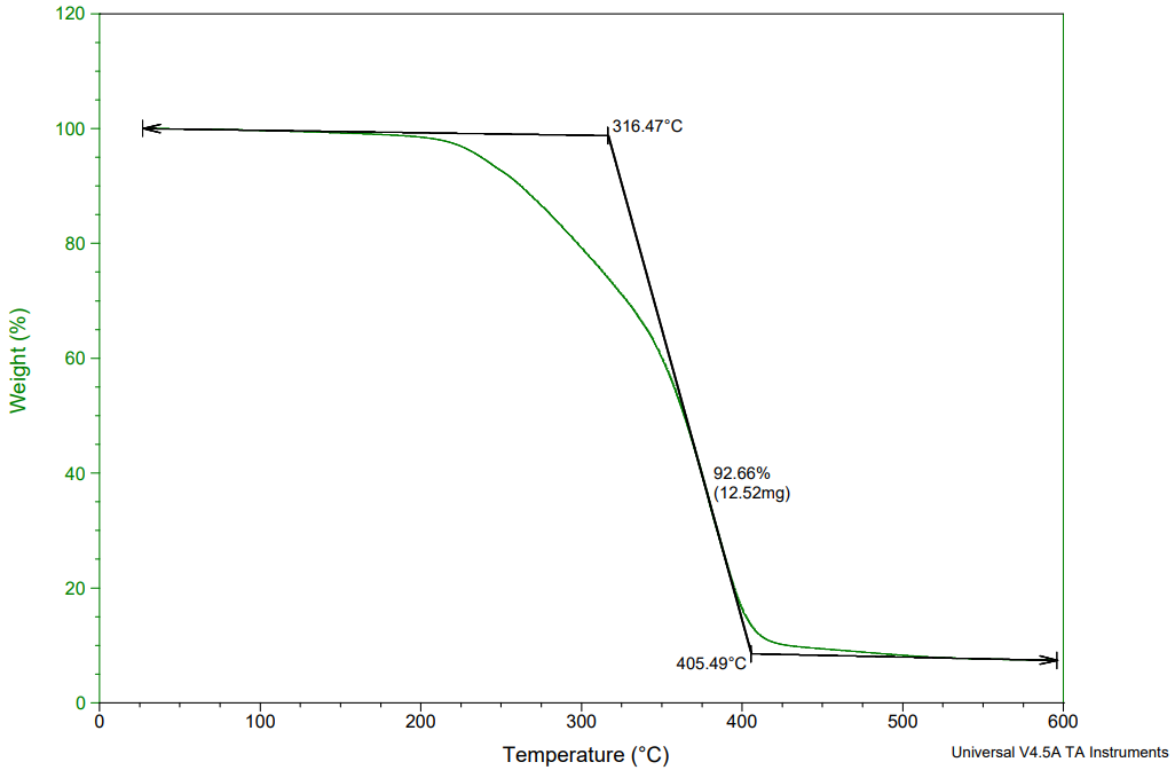

Figure A12. EPL 4 cast specimen 3 TGA results.

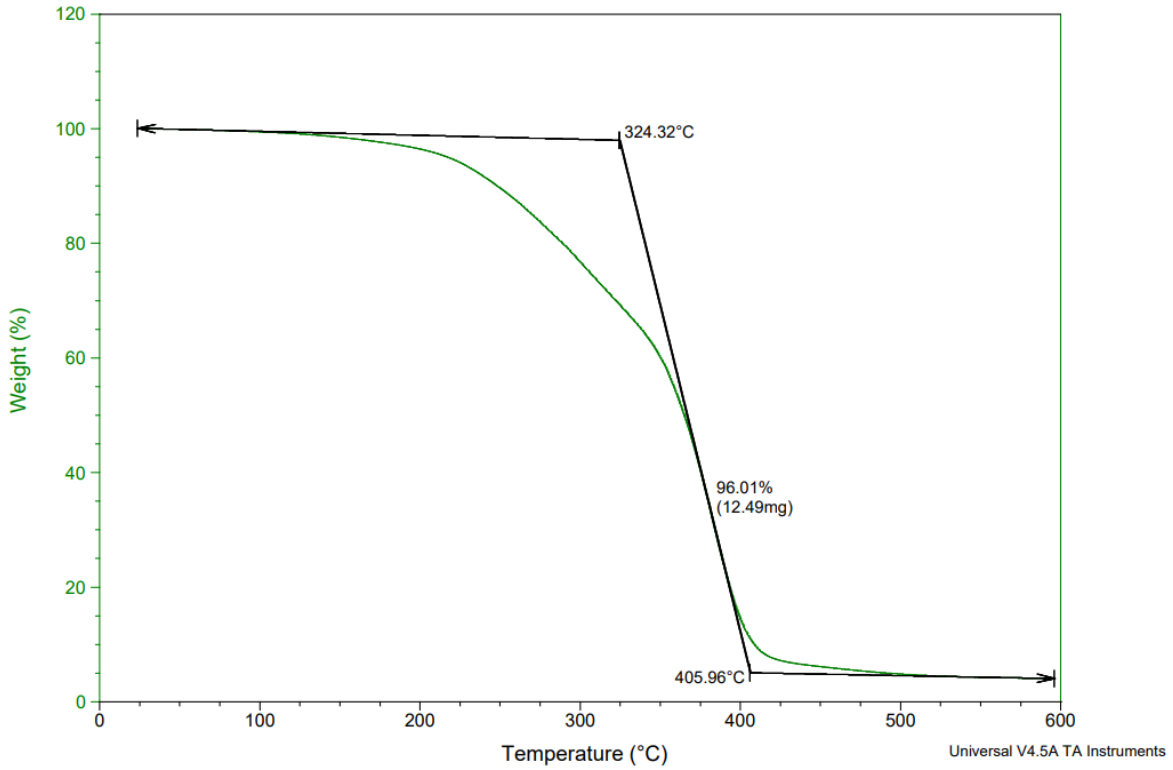

Figure A13. EPL 4 print specimen 1 TGA results.

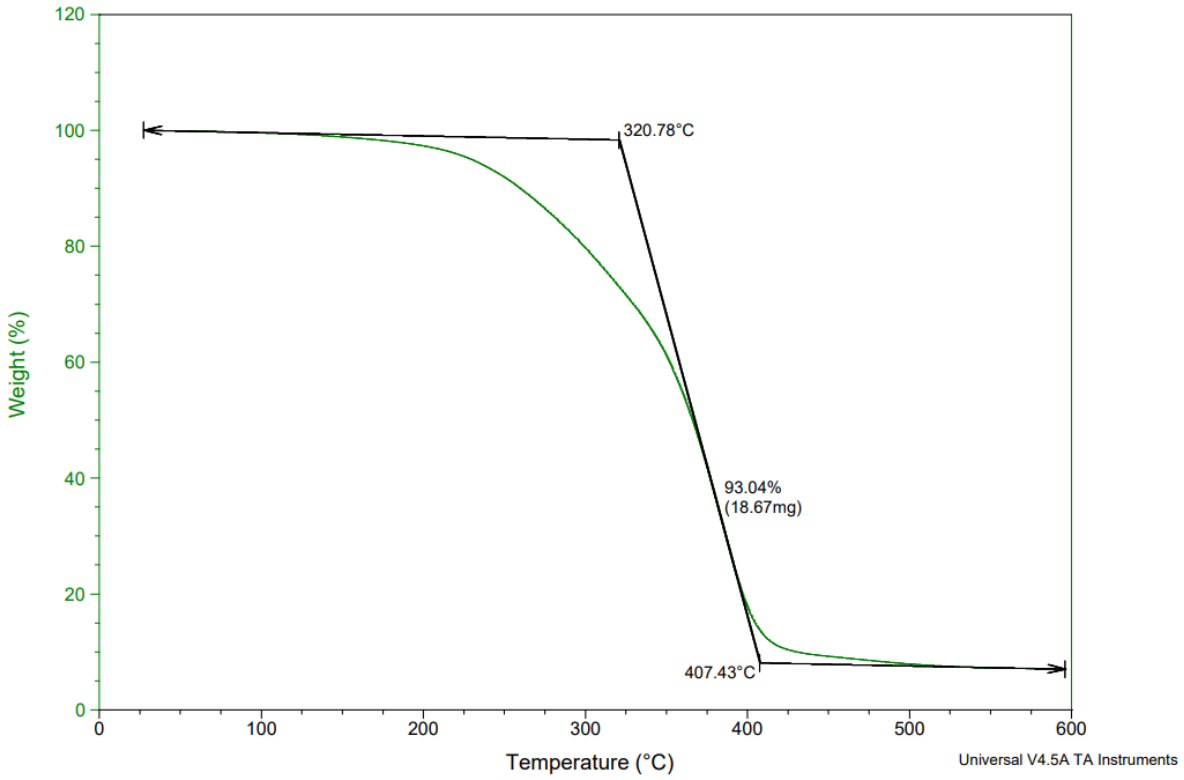

Figure A14. EPL 4 print specimen 2 TGA results.

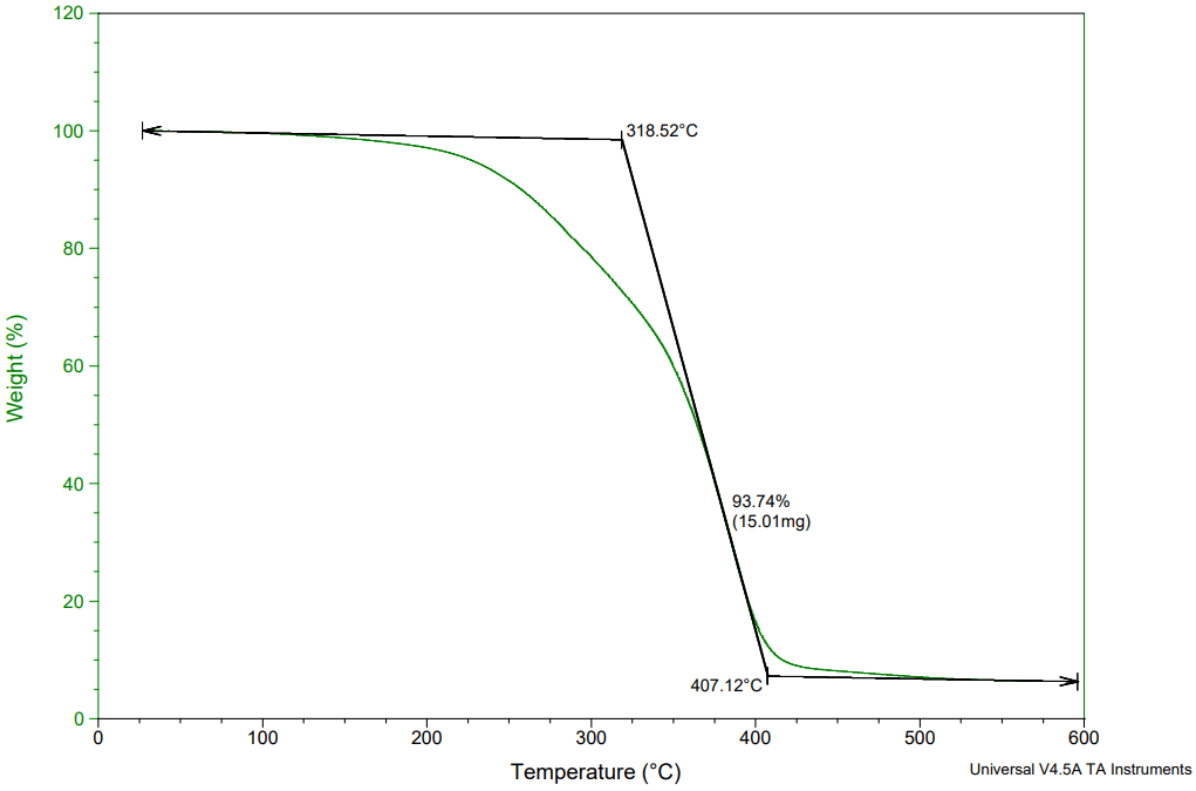

Figure A15. EPL 4 print specimen 3 TGA results.

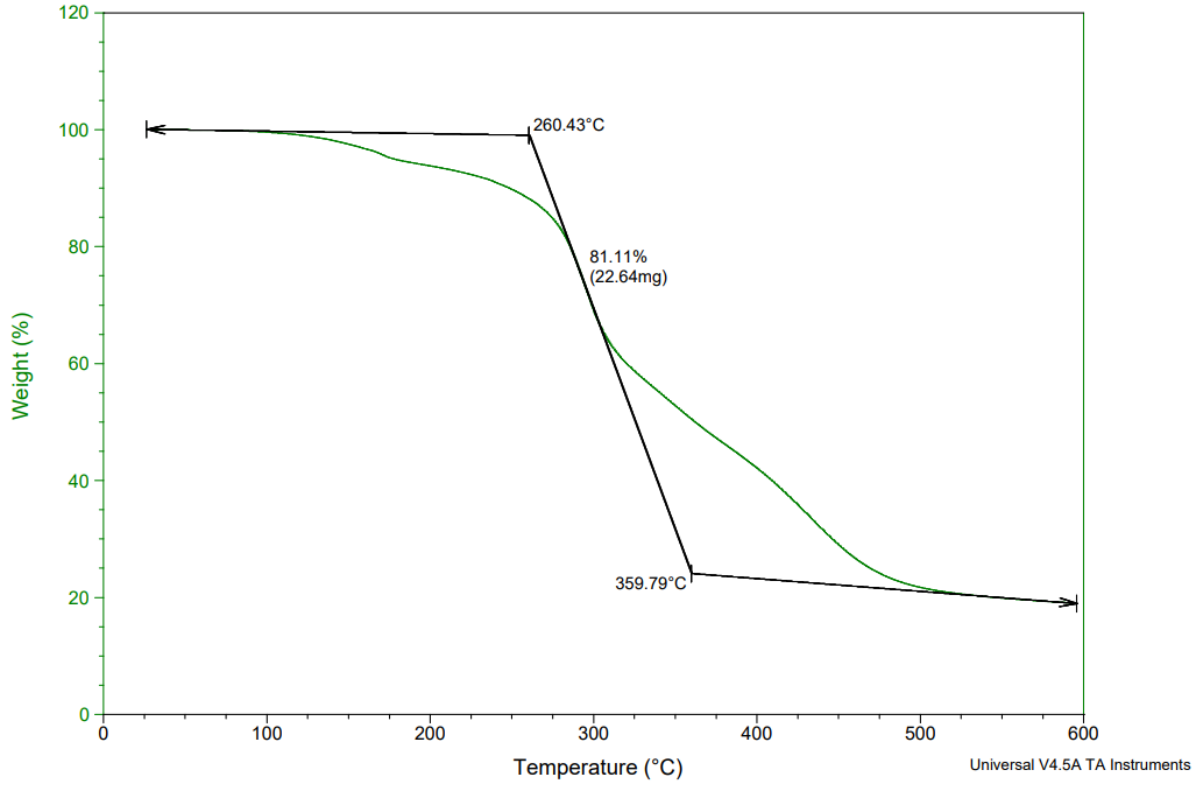

Figure A16. PX cast specimen 1 TGA results.

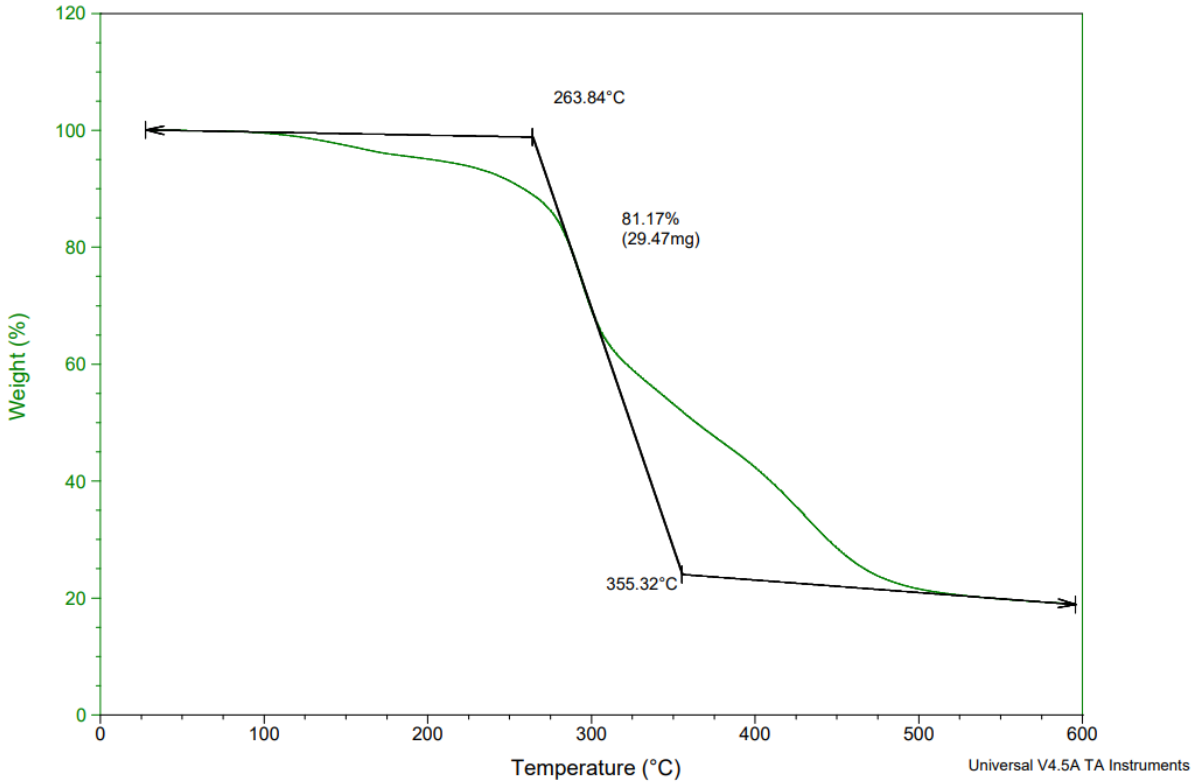

Figure A17. PX cast specimen 2 TGA results.

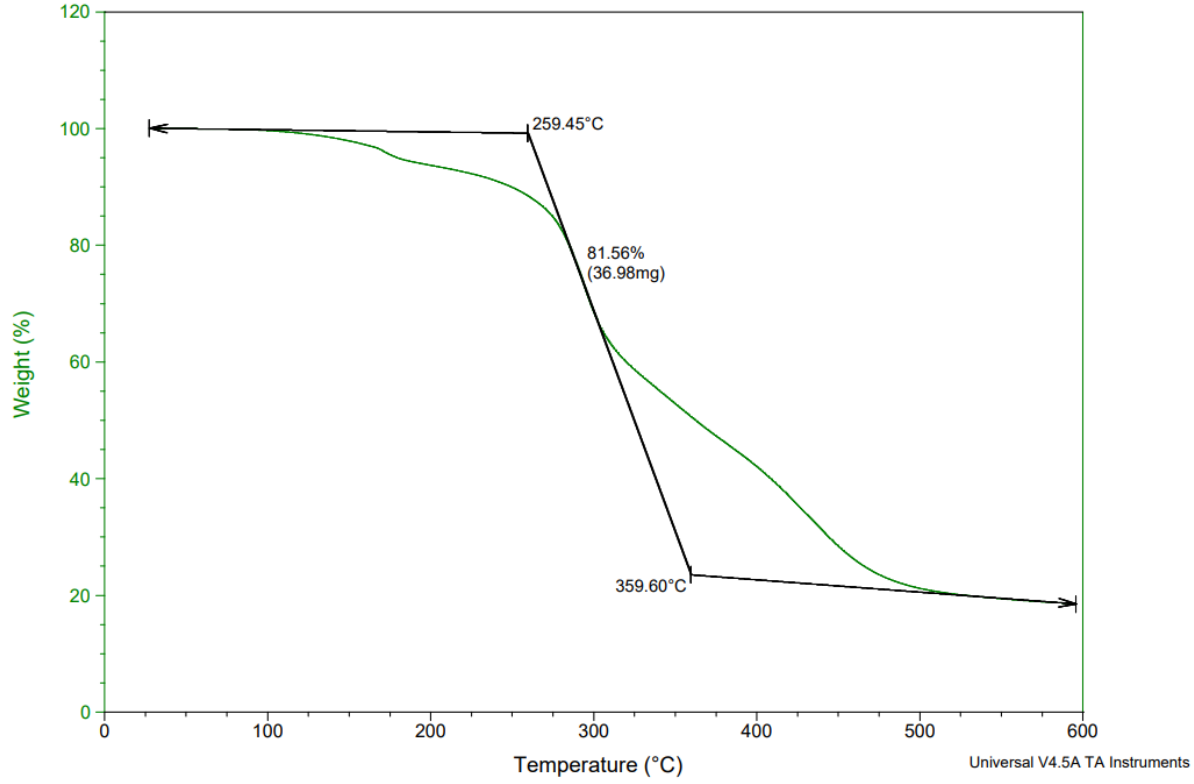

Figure A18. PX cast specimen 3 TGA results.

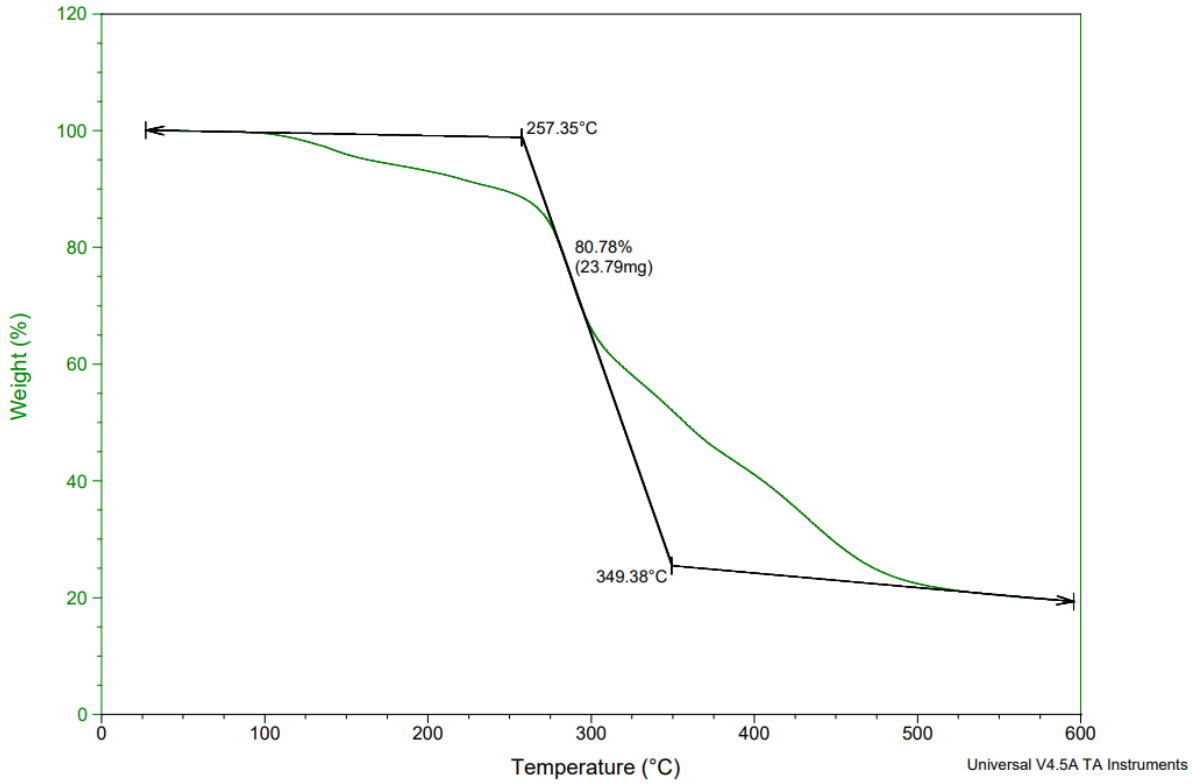

Figure A19. PX printed specimen 1 TGA results.

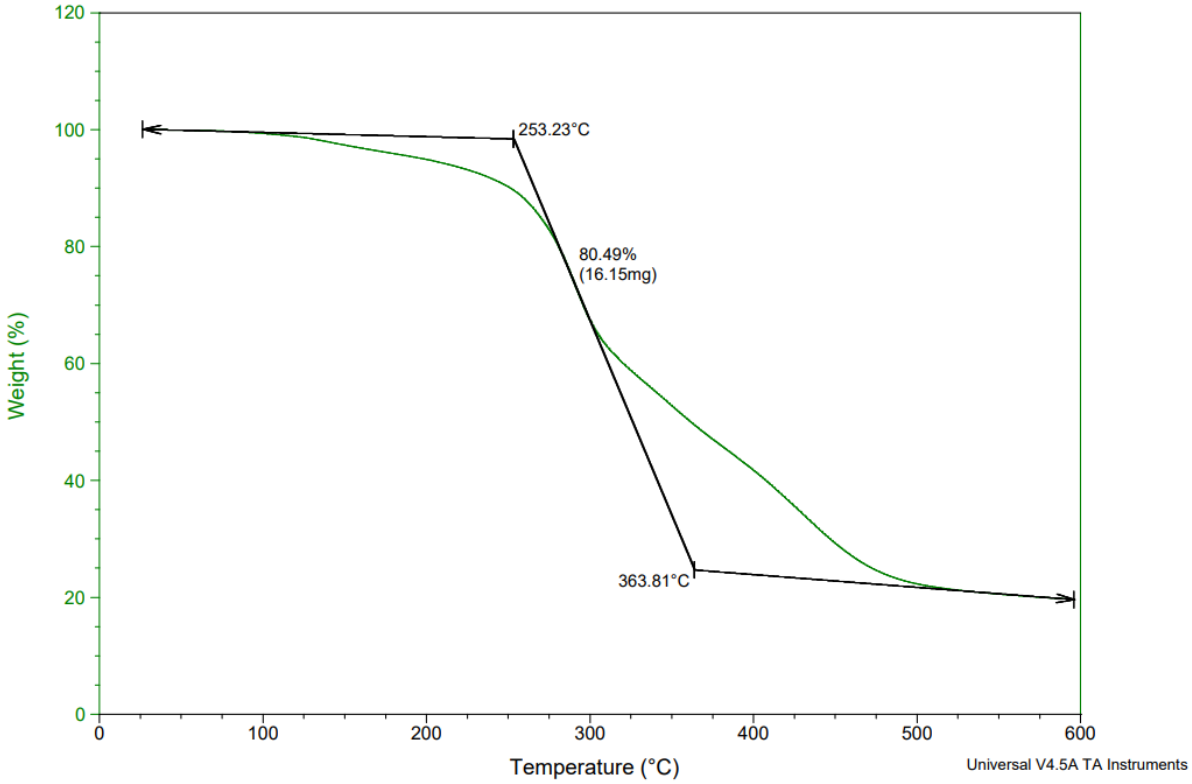

Figure A20. PX printed specimen 2 TGA results.

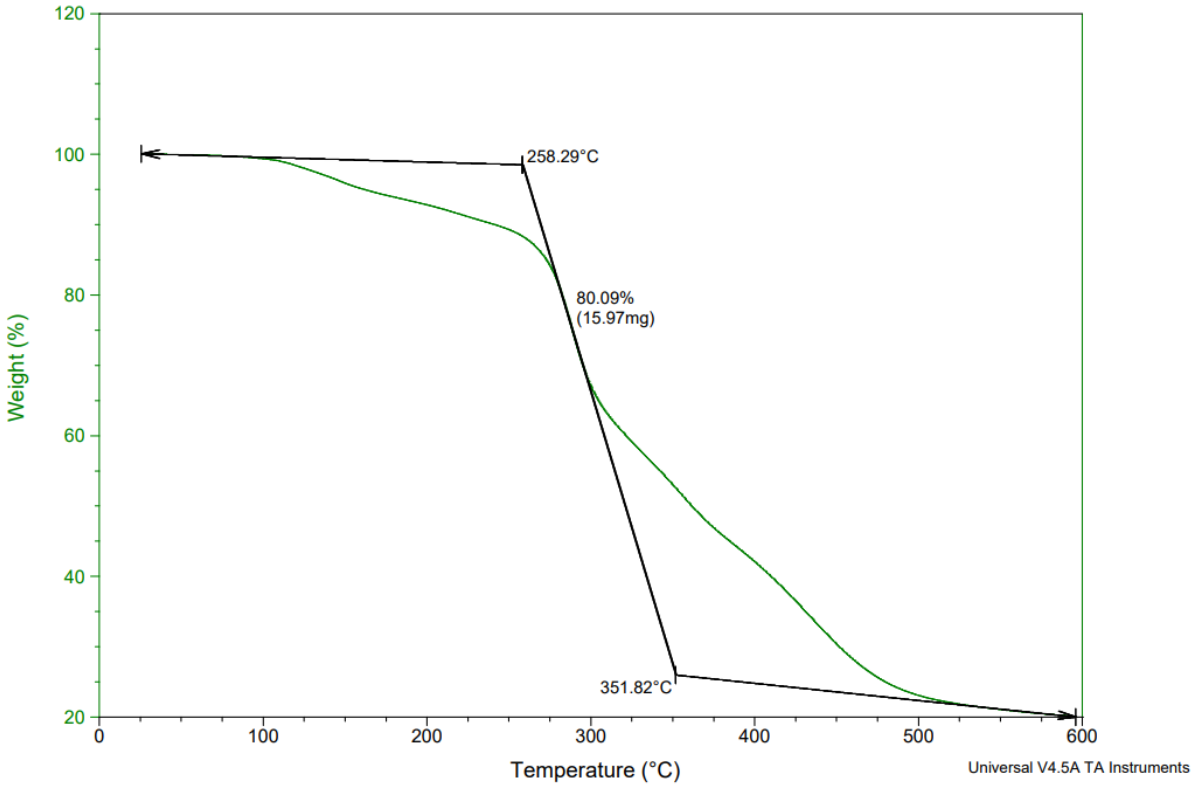

Figure A21. PX printed specimen 3 TGA results.

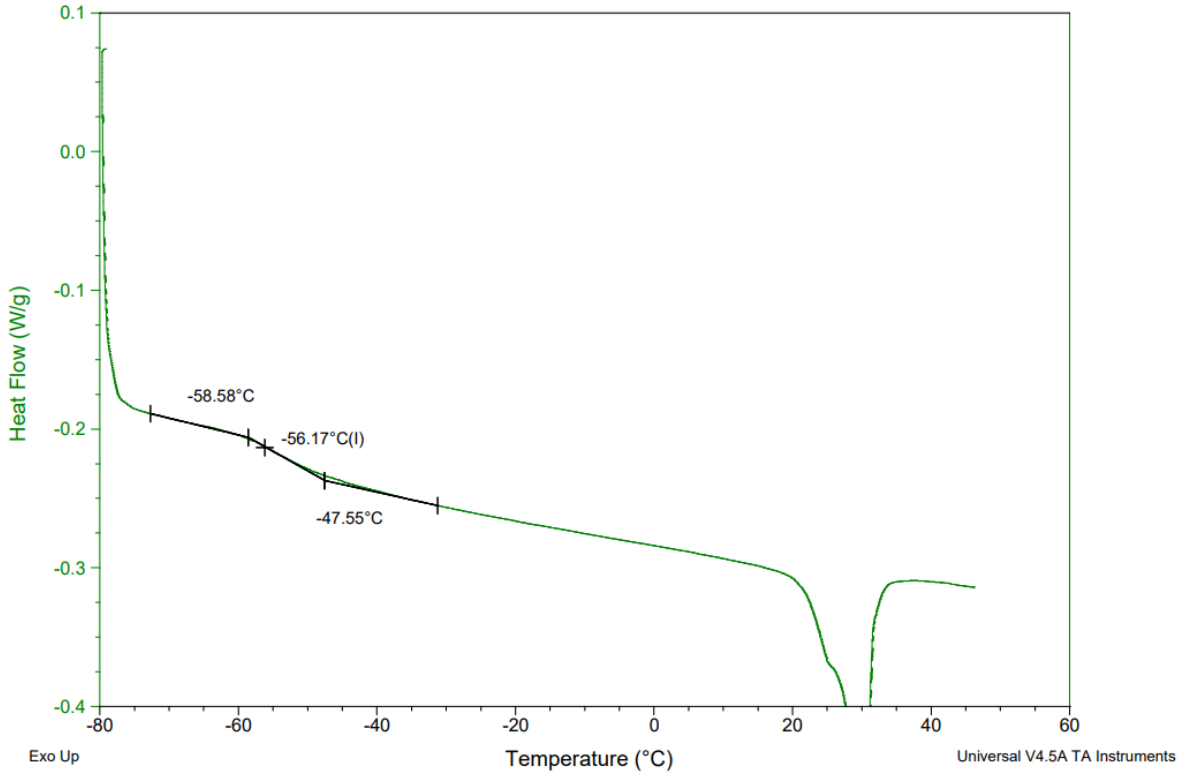

Figure A22. EPL 4 cast specimen 1 DSC results.

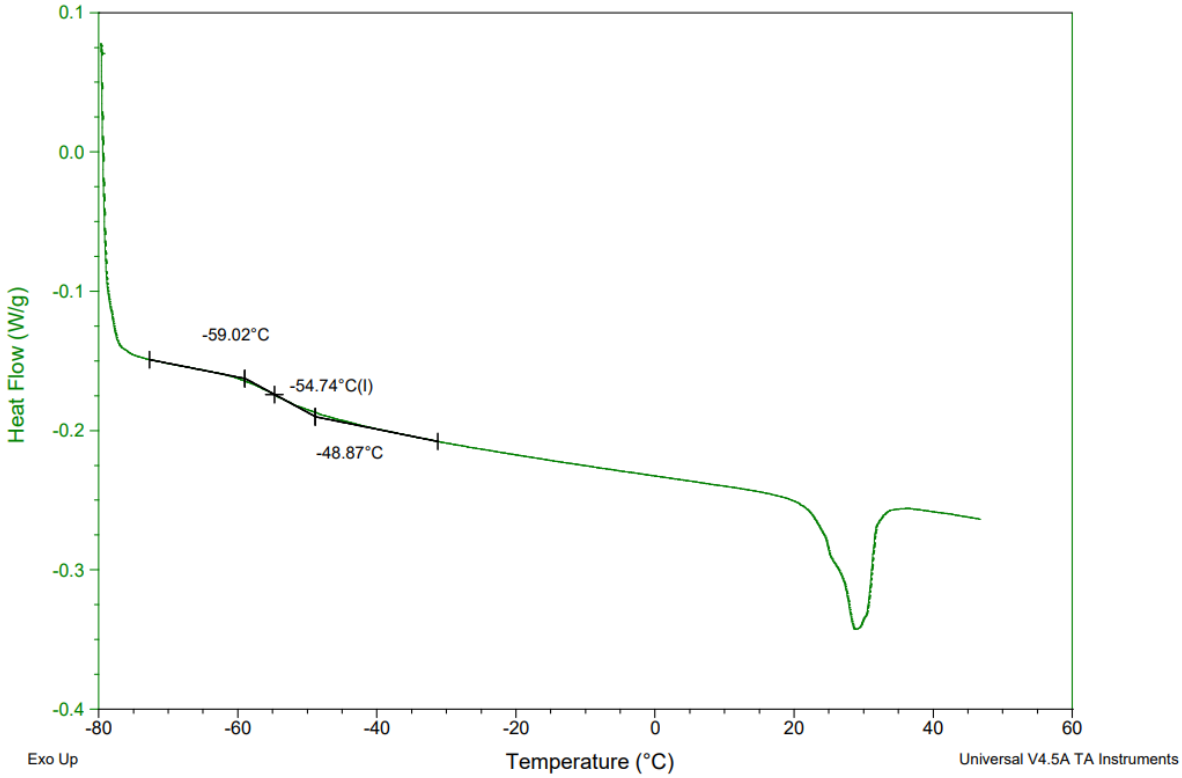

Figure A23. EPL 4 cast specimen 2 DSC results.

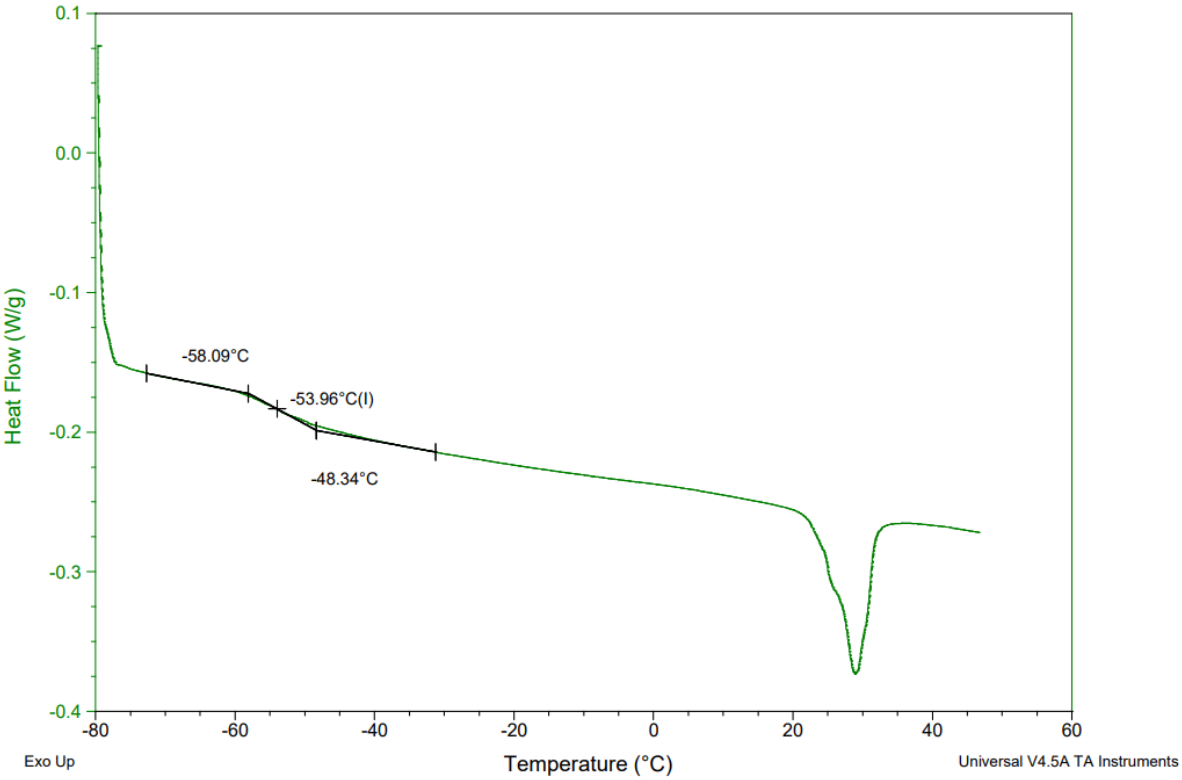

Figure A24. EPL 4 cast specimen 3 DSC results.

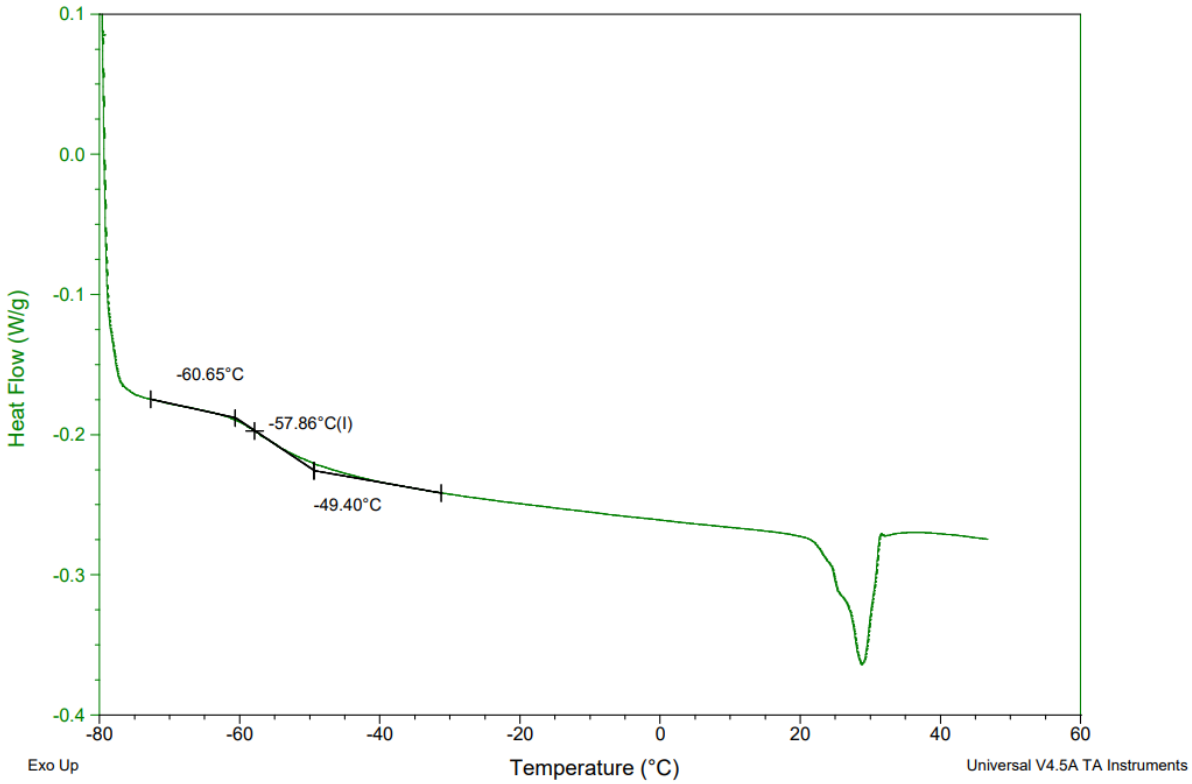

Figure A25. EPL 4 print specimen 1 DSC results.

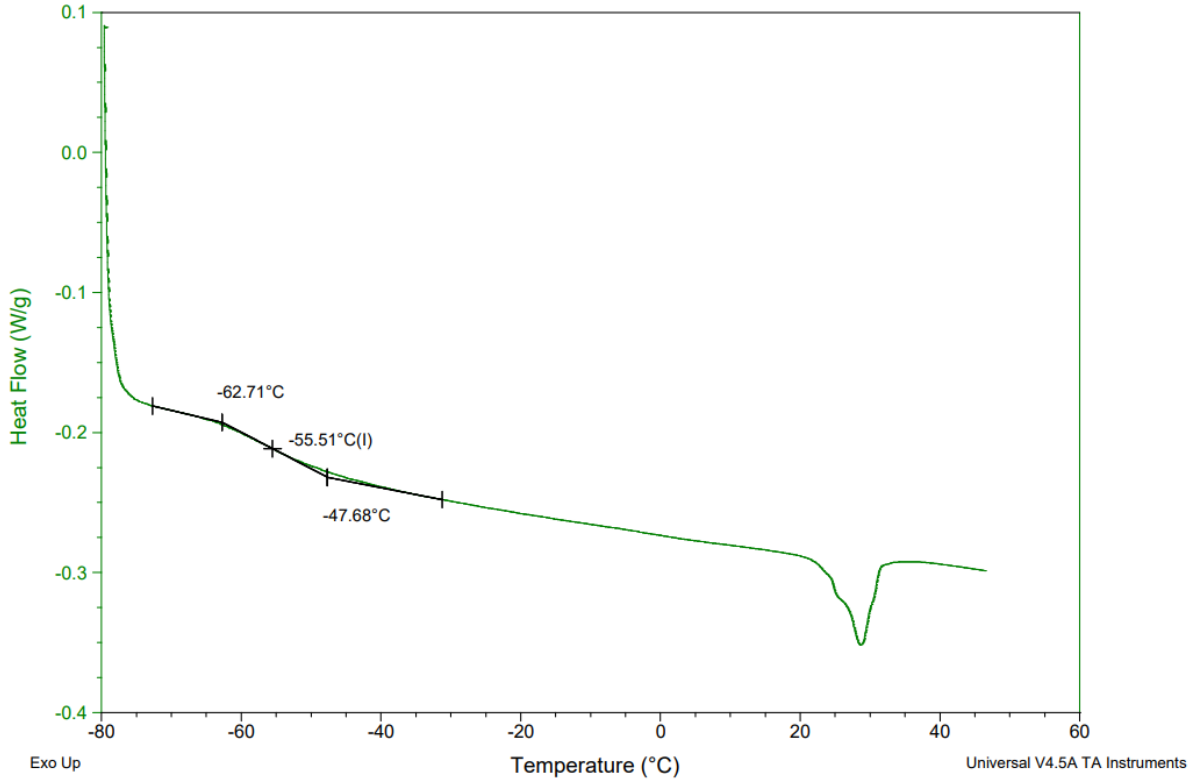

Figure A26. EPL 4 print specimen 2 DSC results.

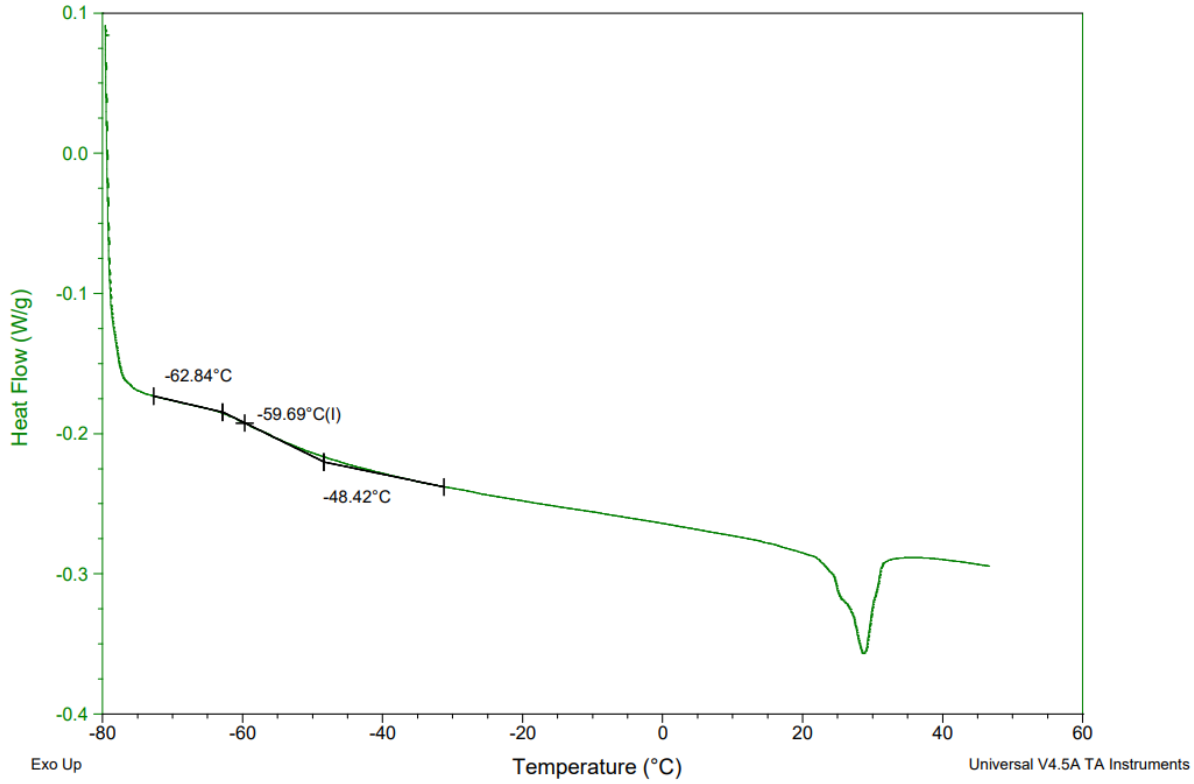

Figure A27. EPL 4 print specimen 3 DSC results.

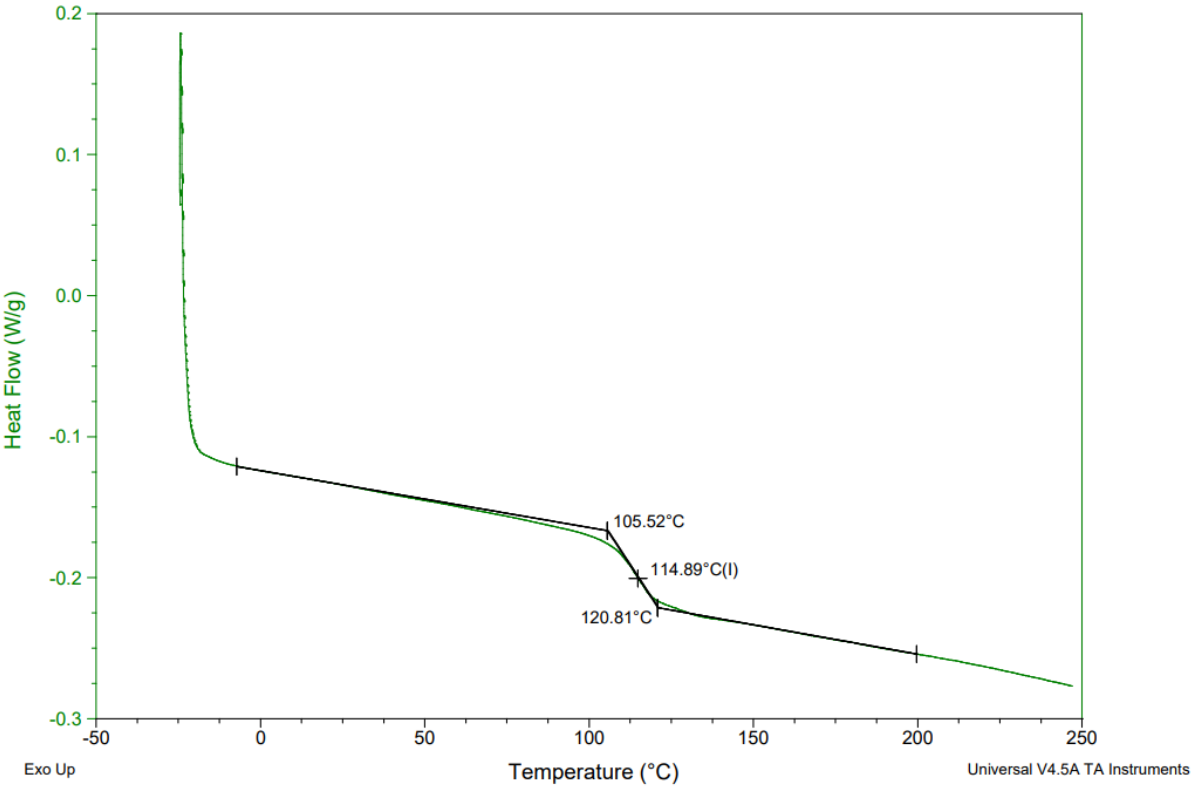

Figure A28. PX cast specimen 1 DSC results.

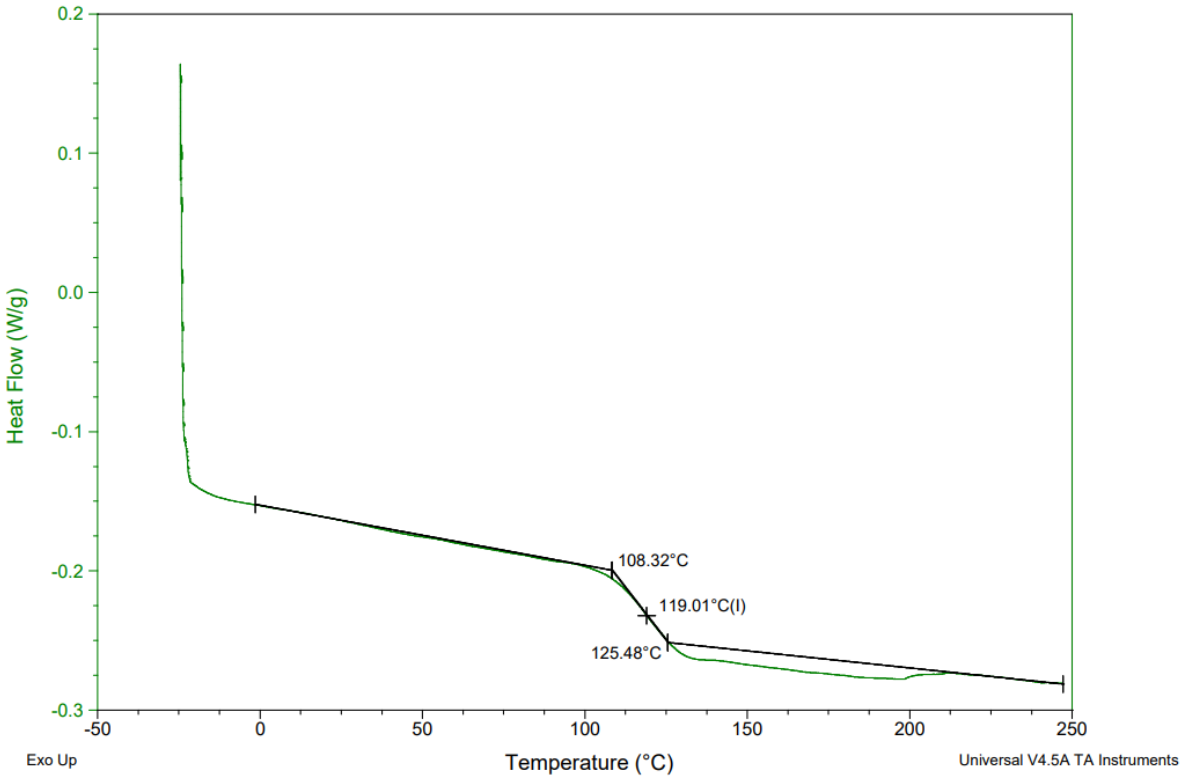

Figure A29. PX cast specimen 2 DSC results.

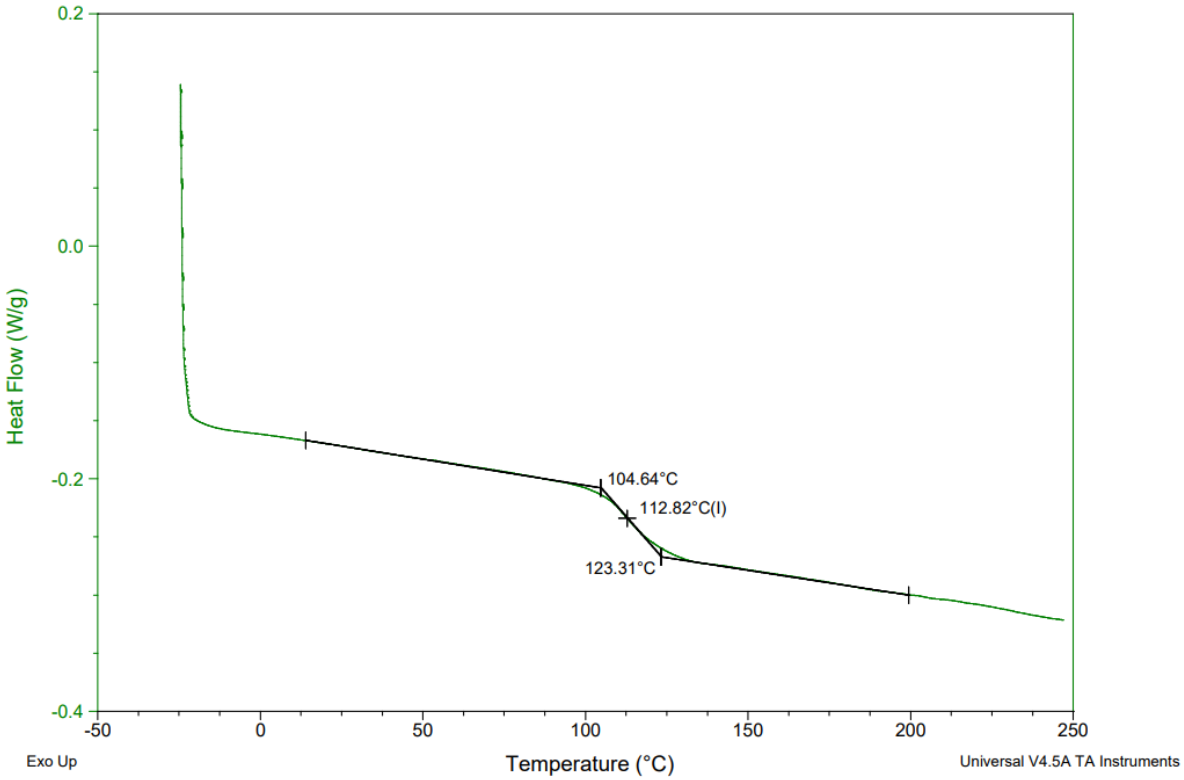

Figure A30. PX cast specimen 3 DSC results.

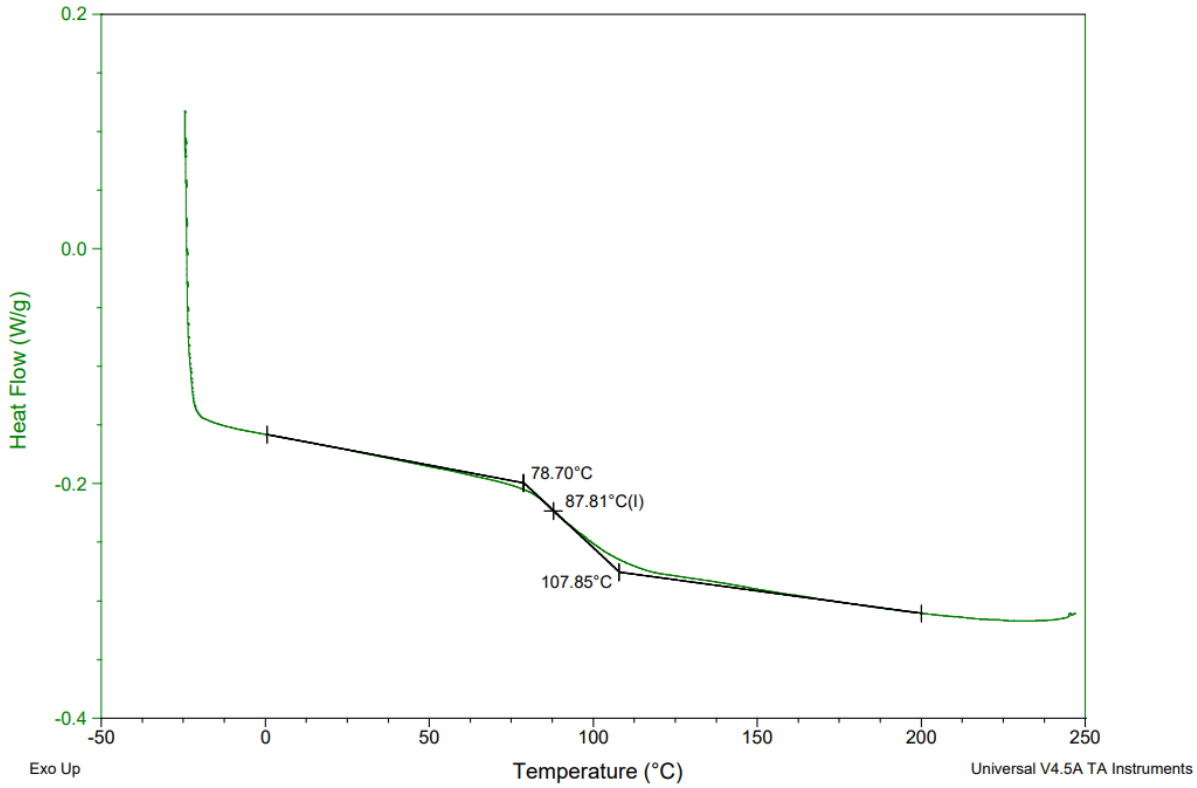

Figure A31. PX printed specimen 1 DSC results.

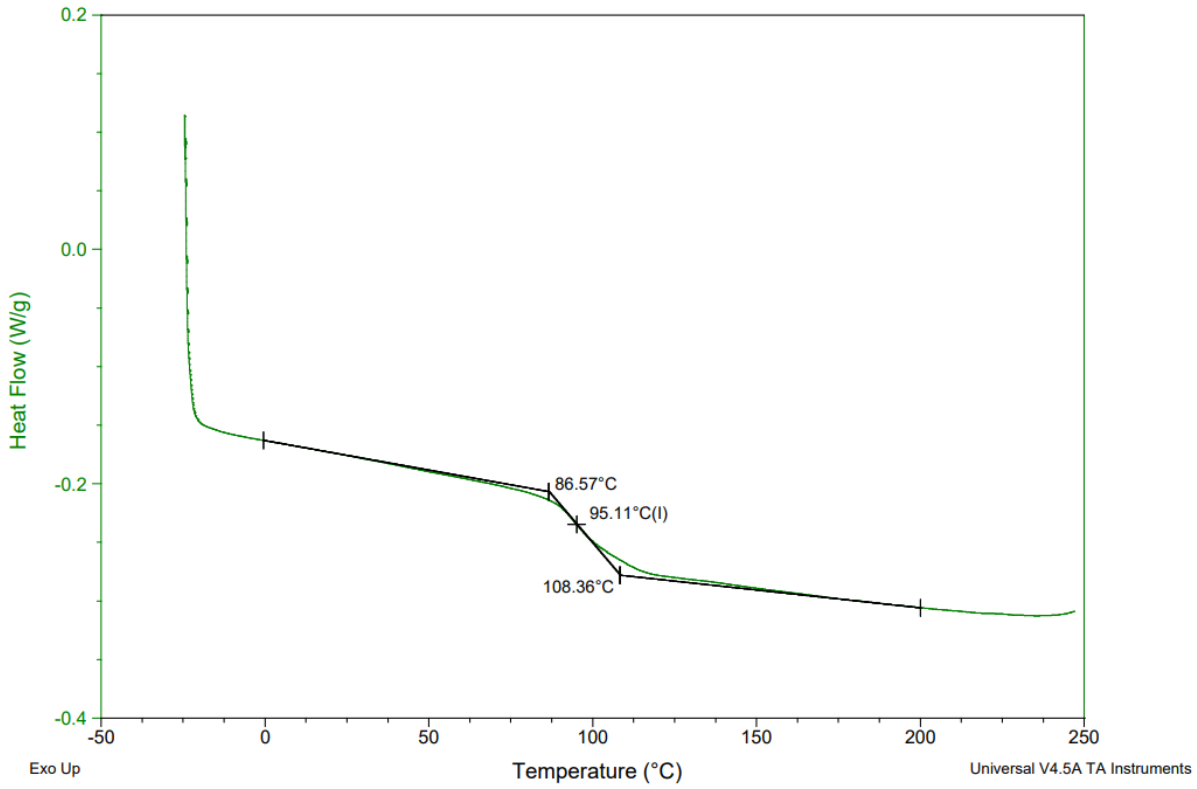

Figure A32. PX printed specimen 2 DSC results.

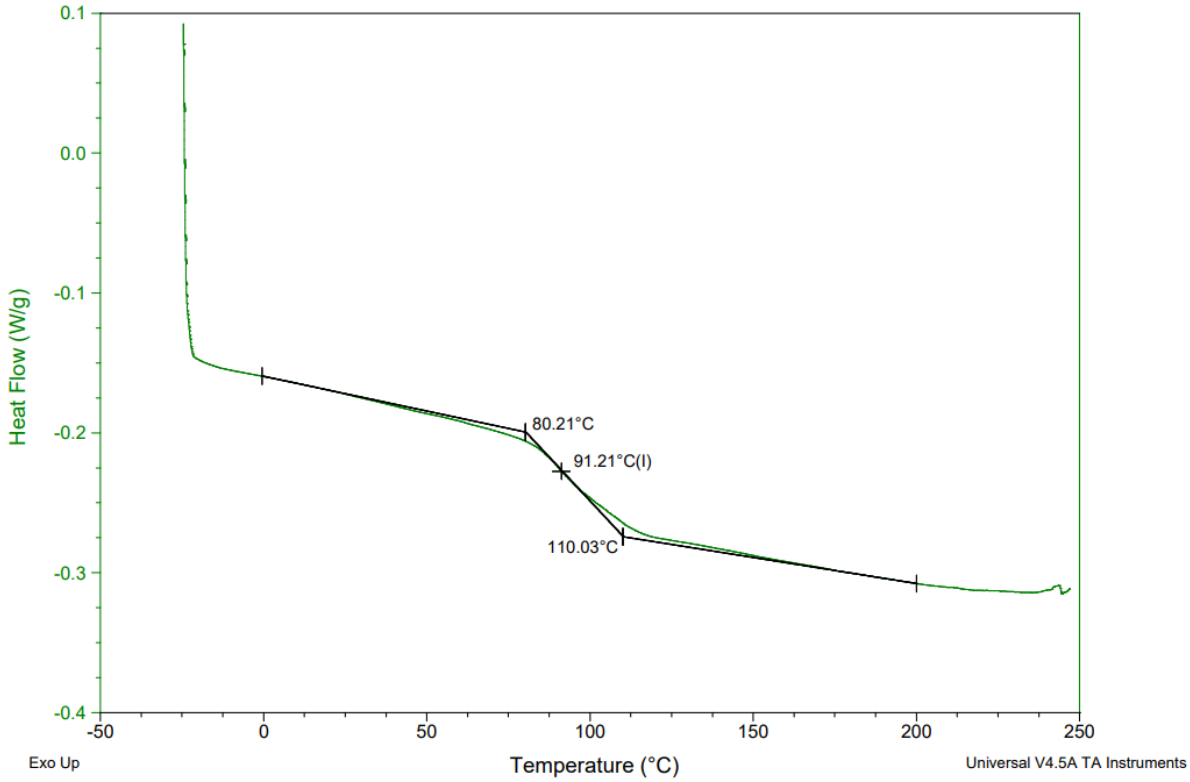

Figure A33. PX printed specimen 3 DSC results.